Rapid post-glacial bedrock weathering in coastal Norway

Jane Lund Andersen [a,b,*], Annina Margreth [a], Ola Fredin [c], Henriette Linge [d,e],
Bradley W. Goodfellow [f], Johan C. Faust [g], Jochen Knies [a,h], Terje Solbakk [a], Edward J. Brook [i],
Thomas Scheiber [j], Roelant van der Lelij [a], Valentin Burki [k], Lena Rubensdotter [a,l], Tobias Himmler [a],
Serdar Yeşilyurt [m,n], Marcus Christl [o], Christof Vockenhuber [p], Naki Akçar [m]

[a] Geological Survey of Norway, Leiv Eirikssons vei 39, 7040 Trondheim, Norway
[b] Department of Geoscience, Aarhus University, Høegh-Guldbergsgade 2, 8000 Aarhus C, Denmark
[c] Department of Geoscience and Petroleum, Norwegian University of Science and Engineering (NTNU), NO-7491 Trondheim, Norway
[d] Department of Earth Science, University of Bergen, NO-5020 Bergen, Norway
[e] Bjerknes Centre for Climate Research, NO-5020 Bergen, Norway
[f] Geological Survey of Sweden, Kiliansgatan 10, 22350 Lund, Sweden
[g] MARUM-Center for Marine Environmental Sciences, University of Bremen, Leobener Strasse 8, 28359 Bremen, Germany
[h] CAGE – Centre for Arctic Gas Hydrate, Environment and Climate, University of Tromsø, 9037 Tromsø, Norway
[i] College of Earth, Ocean, and Atmospheric Sciences, Oregon State University, Corvallis, OR 97331, USA
[j] Department of Environmental Sciences, Western Norway University of Applied Sciences, Sogndal, Norway
[k] Rüttenenstrasse 35, CH-4515 Oberdorf, Switzerland
[l] Department of Geology, University Centre of Svalbard (UNIS), NO-9171 Longyearbyen, Norway
[m] Institute of Geological Sciences, University of Bern, Baltzerstrasse 1-3, 3012 Bern, Switzerland
[n] Department of Geography, Ankara University, Sıhhiye, 06100 Ankara, Turkey
[o] Laboratory of Ion Beam Physics (LIP), ETH Zurich, Otto-Stern-Weg 5, 8093 Zurich, Switzerland
[p] Laboratory of Ion Beam Physics (LIP), ETH Zurich, Otto-Stern-Weg 5, 8093 Zurich, Switzerland

ARTICLE INFO

ABSTRACT

Quantifying bedrock weathering rates under diverse climate conditions is essential to understanding timescales of landscape evolution. Yet, weathering rates are often difficult to constrain, and associating a weathered landform to a specific formative environment can be complicated by overprinting of successive processes and temporally varying climate. In this study, we investigate three sites between 59°N and 69°N along the Norwegian coast that display grussic saprolite, tafoni, and linear weathering grooves on diverse lithologies. These weathering phenomena have been invoked as examples of geomorphic archives predating Quaternary glaciations and consequently as indicators of minimal glacial erosion. Here we apply cosmogenic nuclide chronometry to assess the recent erosional history. Our results demonstrate that all three sites experienced sufficient erosion to remove most cosmogenic nuclides formed prior to the Last Glacial Maximum. This finding is inconsistent with preservation of surficial (<1–2 m) weathered landforms under non-erosive ice during the last glacial period, while simultaneously demonstrating that post-glacial weathering and erosion rates can be locally rapid (4–10 cm kyr^{-1}) in cold temperate to subarctic coastal locations.

1. Introduction

Bedrock surfaces displaying glacial abrasion features, including striae and chatter marks, are widespread in formerly glaciated regions including Greenland, the Canadian Arctic, Fennoscandia, and Antarctica. The persistence of these mm- to cm-scale indentations through the Holocene shows that post-glacial surface weathering rates in glacially scoured landscapes are often low. For example, numerous measurements of the heights of quartz veins protruding ice-sculpted bedrock across Scandinavia, yield Holocene bedrock erosion rates of 0.005–0.48 cm kyr^{-1} (Dahl, 1967; André, 2002; Nicholson, 2008; Matthews and Owen, 2011). It is therefore unsurprising that formative processes and ages of extensively weathered landforms in cold, formerly glaciated regions have been debated. Blockfields, which often cover high-elevation low-relief mountains summits, have been central to this debate (Ballantyne, 1998; Small et al., 1999; Marquette et al., 2004; Strømsøe and Paasche, 2011; Goodfellow et al., 2014a; Andersen et al., 2019). In addition, the ages of

* Corresponding author at: Geological Survey of Norway, Leiv Eirikssons vei 39, 7040 Trondheim, Norway.
E-mail address: jane.lund@geo.au.dk (J.L. Andersen).

other weathering phenomena such as grussic and clay-rich saprolites (Roaldset et al., 1982; Peulvast, 1985, 1986, 1988; Hall, 1986; Bouchard and Jolicoeur, 2000; Islam et al., 2002; Paasche et al., 2006; Ebert et al., 2012; Olesen et al., 2013; Fredin et al., 2017), as well as a grooved calcareous schist at the coast of southern Norway (Reusch, 1878; Olesen et al., 2013), are a focus of discussion of weathering rates and landform ages in formerly glaciated regions. These weathering phenomena prompt the question of whether they: i) developed post-glacially on late-glacial and Holocene time-scales; ii) developed earlier, and were protected from subsequent glacial erosion either beneath cold-based, non-erosive, ice or on nunataks, during one or more glacial periods, or; iii) represent remnants of thick, pre-Quaternary weathering profiles truncated by glacial erosion.

Constraining the age and formation processes of these weathered landforms has important implications for the interpretation of landscape evolution (Nielsen et al., 2009; Schermer et al., 2017), as well as for understanding the dimensions, basal conditions, and resulting erosional efficiency, of former ice sheets (Lidmar-Bergström, 1997; Paasche et al., 2006; Nesje et al., 2007). Establishing the geomorphic history of weathered landforms in formerly glaciated regions, is thus key to resolving disputes on landscape evolution and glacial erosion efficiency, including on high-latitude passive margins (Staiger et al., 2005; Strømsøe and Paasche, 2011; Steer et al., 2012; Hall et al., 2013; Margreth et al., 2016; Pedersen et al., 2016; Andersen et al., 2018; Pedersen et al., 2021).

In Fennoscandia, suggested formation ages for weathering phenomena such as saprolites, blockfields, and linear weathering grooves, range from Late Proterozoic (Lidmar-Bergström et al., 1997), over Mesozoic (Lidmar-Bergström et al., 1997; Olesen et al., 2013; Fredin et al., 2017), Neogene (Reusch, 1878; Roaldset et al., 1982; Paasche et al., 2006; Strømsøe and Paasche, 2011), to Plio-Pleistocene timescales (Lidmar-Bergström et al., 1997; Goodfellow et al., 2014a; Andersen et al., 2018). For grussic saprolites, the suggestion of pre-Cenozoic ages is often coupled to the notion that they constitute the least altered basal parts of initially very deep (>100 m) pre-glacial weathering profiles (Roaldset et al., 1982; Islam et al., 2002; Paasche et al., 2006; Olesen et al., 2013). The contrasting age estimates largely hinge on the difficulty of dating the weathering products, and on the observed low weathering rates in cold temperate to arctic climates (Dahl, 1967; André, 2002; Nicholson, 2008; Matthews and Owen, 2011; Olesen et al., 2013). In the absence of a stratigraphic age control on the weathering phenomena, the attribution of their formation to pre-glacial climates primarily rests on the assumption that Quaternary chemical weathering rates are very low, and that clay minerals such as kaolinite and gibbsite do not form in cold climates (Roaldset et al., 1982; Islam et al., 2002; Paasche et al., 2006; Strømsøe and Paasche, 2011). Several cosmogenic nuclides studies have shown, however, that blockfields mantling some Scandinavian mountains comprise Quaternary regoliths (Goodfellow et al., 2014a; Andersen et al., 2019; Jansen et al., 2019). In this study, we investigate three coastal localities in Norway that display three distinct types of weathering (saprolitisation, and the sculpting of tafoni and linear weathering grooves) developed in varying lithologies and climatic settings (Fig. 1). The formation of these weathering features, at the investigated sites or at similar nearby localities, was previously considered to have initiated during past warmer climates and, by inference, to have undergone limited subsequent glacial erosion (Reusch, 1878; Roaldset et al., 1982; Peulvast, 1985, 1986; Paasche et al., 2006; Strømsøe and Paasche, 2011). Here, we apply cosmogenic nuclide chronometry to show that all three sites were eroded to a depth of at least 1–2 m during the last glacial period. This demonstrates that surficial weathering features must have formed post-glacially at locally significant rates in cold temperate to subarctic coastal climates.

2. Site descriptions

2.1. Bogvetten – saprolite

Saprolites are scattered across Fennoscandia (Lidmar-Bergström et al., 1995; Olesen et al., 2012; Fredin et al., 2017) and are particularly prominent on the Arctic islands and the coastal region of mainland Norway proximal to the Lofoten-Vesterålen archipelago (Fig. 2a) (Peulvast, 1985, 1986; Paasche et al., 2006; Strømsøe and Paasche, 2011; Olesen et al., 2013). The chemical weathering of saprolites in this region varies from extensive clay formation to only slight alteration of the parent rock, resulting in both clayey and grussic saprolites (Sturt et al., 1979; Lidmar-Bergström et al., 1995; Paasche et al., 2006; Olesen et al., 2013). The saprolites occur in settings ranging from mountain tops (Nesje et al., 2007; Strømsøe and Paasche, 2011) to outcrops in glacial valleys that are often associated with faults and fracture zones (Olesen et al., 2013). The saprolite thicknesses in the region vary from a few centimetres to tens of meters on the islands of Hadseløy (68°32′ N, 14°53′E, 150 m a.s.l.) and Hamarøy (68°3′N, 15°26′E, 25 m a.s.l.; Olesen et al., 2012). There are generally few independent age estimates of these saprolites, although they are sometimes found beneath, or incorporated into, glacial till indicating that they predate at least the last glacial period (Olesen et al., 2012). At Ramså on Andøya (Fig. 2a), a clayey saprolite developed in gneiss is overlain by Jurassic and Cretaceous sediments showing that this saprolite predates the Jurassic (Sturt et al., 1979; Olesen et al., 2012). The proximity of offshore Mesozoic sediments to other saprolites in the area (Fig. 2a; Bøe et al., 2010), opens the question of whether (some of) these saprolites could be pre-Mesozoic saprolites that were first protected beneath sedimentary cover rocks and later truncated by Quaternary glacial erosion (Olesen et al., 2012). Tightening the age constraints on different saprolite types (clayey/grussy) in the area will thus help to clarify the tectonic and geomorphic history of the region.

The mountain summit of Bogvetten (68.21°N, 16.01°E, 521 m a.s.l.) on the coastal mainland of northern Norway (Figs. 2b and 3) is mantled by grussic saprolite, developed in middle to coarse grained dioritic to granitic gneiss (Sigmond, 1992). The Bogvetten saprolite is distinctive because it hosts hundreds of weathered rock pedestals capped by mostly sub-horizontal (but sometimes dipping up to 85°) surfaces of the local gneiss (Fig. 4a). The pedestal surface areas are typically <1–2 m², and they protrude 0.1–1.5 m above the surrounding grussic saprolite. The accordance of adjacent perched rock surfaces indicates that they are remnants of a formerly continuous, undulating, bedrock surface, which has been dissected by processes of weathering and erosion (Figs. 4a, c–e; 5). Although the pedestals are also weathered, to the extent that samples of constituent rock easily disintegrate, their prominence indicates that they have eroded more slowly than the surrounding grussic saprolite. It appears that the bedrock surface that preceded weathering, and which is locally preserved on pedestals, was glacially eroded (Fig. 5a). Whereas glacial polish, striae, and chatter marks were not observed directly on the pedestals, some pedestals have forms consistent with glacial sculpting (Figs. 4e, 5). In addition, ice-sculpted bedrock with chatter marks was observed on bedrock surfaces immediately surrounding the grussy saprolite (Fig. 4g). Abundant grus outwash occurs in ephemeral streams incising the mountain, which indicates that the grus is easily eroded through hillslope creep and fluvial wash (Fig. 4b, f; Supp. Fig. 1a). On the mountain flanks and in adjacent valleys, grussic saprolite is exposed in 2–5-meter-thick sections in roadcuts and within an aggregate quarry (Fig. 2b). The saprolite exposed in these sections is heterogeneous, being restricted to 5–20 cm-thick sharply-bounded bands of weathering along sub-horizontal joints in some places (Fig. 6c), surrounding corestones in other places (Fig. 6b, d), and being continuous to depths of several meters in other locations (Fig. 6a).

During the last glaciation, Bogvetten was situated ~200 km inland of the LGM ice-margin at the shelf break (Fig. 1), close to the head of the

Fig. 1. Overview map of localities in Norway. ETOPO1 elevation model (NOAA National Geophysical Data Center, 2009). Last Glacial Maximum (LGM) and Younger Dryas (YD) ice margins (Stroeven et al., 2016).
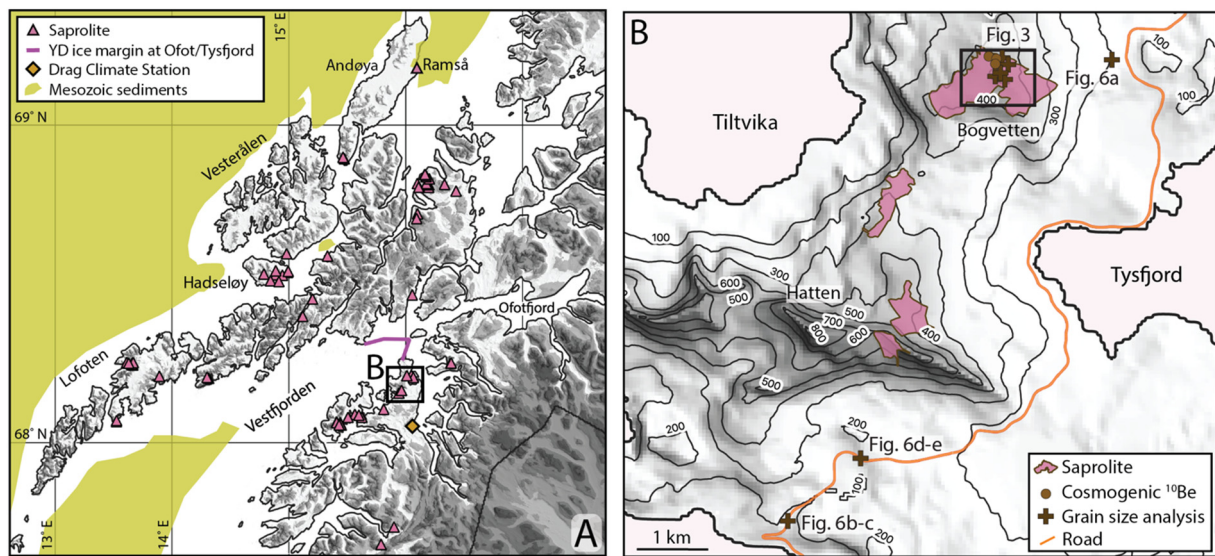

Fig. 2. A) Saprolite occurrences in the Lofoten-Vesterålen region (Peulvast, 1986; Paasche et al., 2006, Olesen et al., 2012; Oddbjørn Kløvjan pers. comm. June 2020). Younger Dryas (YD) ice margin position at the bathymetric thresholds of Ofot- and Tysfjorden after Fløistad et al., 2009. Extent of Mesozoic sediments after Bøe et al., 2010. B) Mapped extent of saprolite in the vicinity of Bogvetten and sample locations for grainsize and cosmogenic [10]Be analysis.
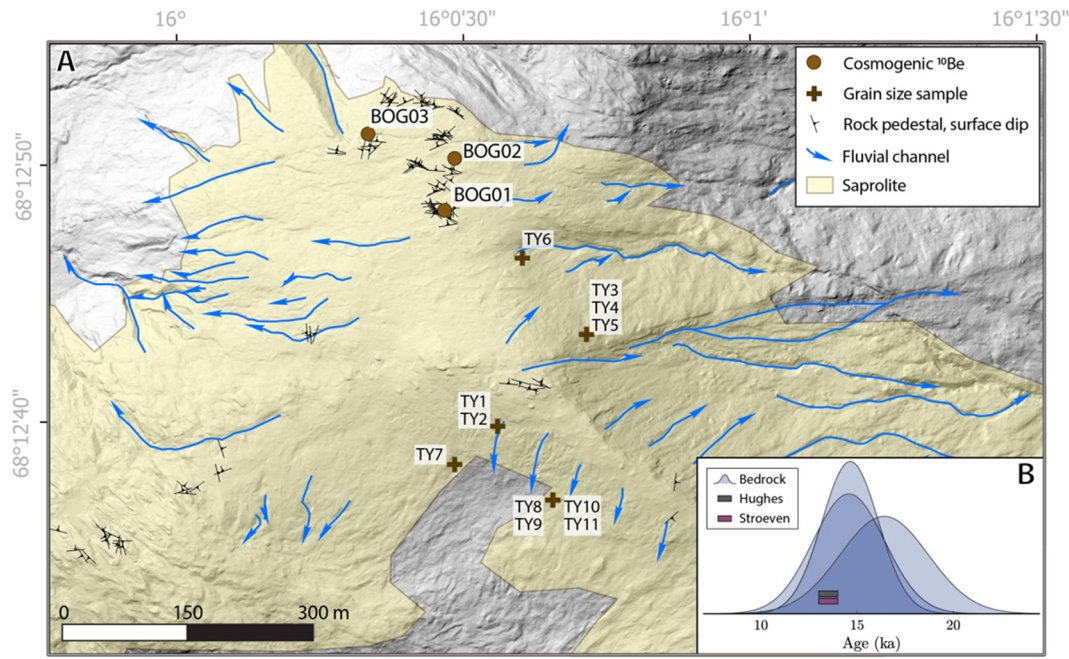
Fig. 3. A. Saprolite extent at Bogvetten and location of samples for [10]Be dating and grain size analysis. B. Probability density functions (camel plots) of cosmogenic [10]Be ages from the three bedrock samples at Bogvetten compared to regional deglaciation estimates by Hughes et al. (2016) and Stroeven et al. (2016).

Vestfjorden Ice Stream (Ottesen et al., 2005). Reconstructions of the collapse of the last Scandinavian Ice Sheet show that the ice sheet margin retreated from the region around Bogvetten at ~13–14 ka (Knies et al., 2007; Hughes et al., 2016; Stroeven et al., 2016). During the Younger Dryas (~12.9–11.7 ka) the ice-sheet margin re-

advanced to a position just north of Bogvetten at the Ofotfjorden and Tysfjorden bathymetric thresholds (Fig. 2a; Olsen, 2002; Fløistad et al., 2009). It is unknown whether the mountain summit (521 m a.s.l.) was briefly re-covered by the Younger Dryas ice sheet re-advance. Considering the short lateral distance (<7 km) to the

Fig. 4. Photographs from Bogvetten. A) Rock pedestals protruding above the eroded saprolite. Note the accordance of the rock surfaces capping the pedestals. B) Grussic saprolite surrounding the summit ridge of Bogvetten. C) and D) Enhanced weathering and erosion in bedrock joints and sampling of cosmogenic nuclide sample BOG02 (c) and BOG01 (d). E) Sample site of BOG03. Note the glacial sculpting of the remnant bedrock surface at this site. F) Ephemeral streams on several sides of Bogvetten incise 2–10 m deep, narrow gorges into saprolite, exposing competent bedrock at their bases. G) A sequence of chatter marks indented into a bedrock surface adjacent to saprolite near Tiltvika.
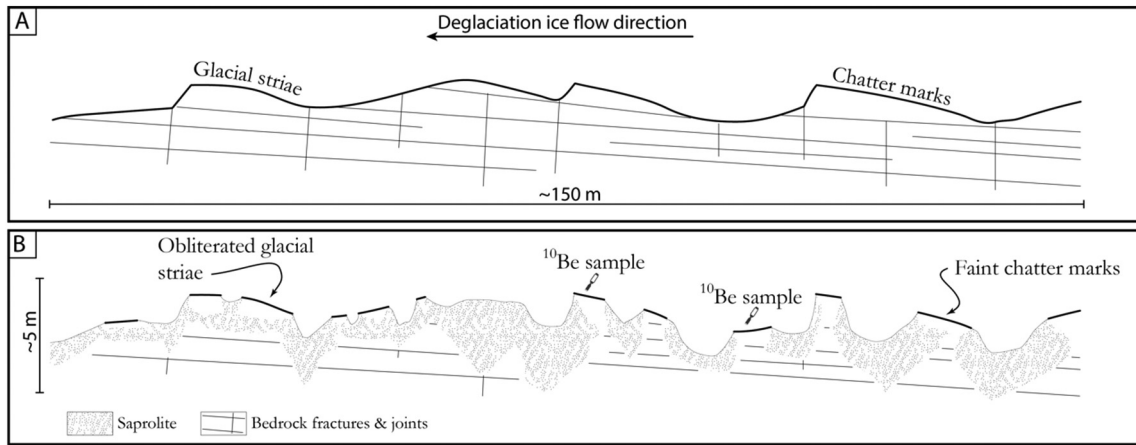
Fig. 5. Conceptual figure of pedestal formation at Bogvetten. A. Glacially sculpted surface prior to saprolitisation. B. Present-day weathered and eroded surface with fragments of the glacially sculpted surface preserved on pedestals. Note that the sketch is not true to scale.

Younger Dryas ice-front position in the fjord this might not be the case.

Following deglaciation of Bogvetten, the late-glacial climate was cold with high-arctic conditions prevailing on Andøya (Alm, 1993) and mean July temperatures ~7–8 °C colder than present (Birks et al., 2014). This was followed by a ~3–4 °C amelioration in Allerød (~13.9–12.9 ka BP) and a few degrees cooling in late Younger Dryas, before July temperatures rose to present levels by about 9.7 cal ka BP (Birks et al., 2014). Holocene temperatures from a northern Norway speleothem record indicate that temperatures were near, or warmer than, present since ~8.5 ka, but with a number of cold excursions including the Little Ice Age (Lauritzen and Lundberg, 1999). The lower altitudinal limit of sporadic permafrost in coastal northern Norway is today at 1200 m a.s.l. (Gisnås et al.,
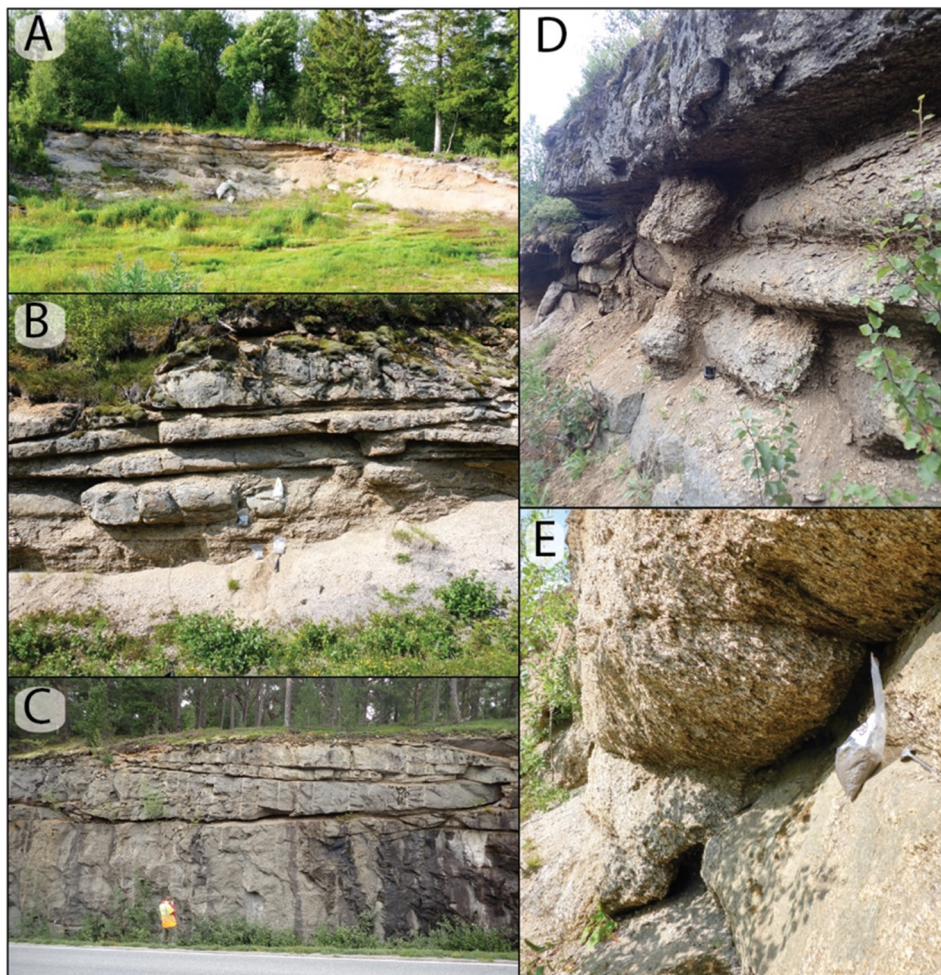

Fig. 6. Saprolite exposed in an aggregate quarry (A) and roadcuts (B-E) near Bogvetten. For locations see Fig. 2b. Samples collected for grainsize analysis from A-B, D (saprolite), and E (fracture plane).

2017), and permafrost probably did not occur below 500 m a.s.l. during the Holocene (Lilleøren et al., 2012).

The present-day mean annual air temperature (MAT) at Bogvetten is 3 °C, mean annual precipitation (MAP) is ~1500 mm (www.senorge.no; www.met.no), and the climate is subpolar oceanic (Köppen, 1936). Mean daily temperature variations at nearby Drag Climate Station (Fig. 2a; 68.02°N, 16.04°E, 19 m a.s.l., 1956–1972 record) fluctuate mostly between −13.7 and 19.4 °C (1st-99th percentile). Precipitation is distributed throughout the year with the driest months (April–May) receiving roughly half the precipitation of the wettest (September–October). Snow typically covers the ground between October and April, reaching maximum depths of ~50–100 cm (www.senorge.no).

2.2. Kråkenes – tafoni and saprolite

The island Vågsøy on the outermost Atlantic coast in west-central Norway features both cavernous weathering forms and saprolites (Fig. 7a, b). We follow Groom et al. (2015) and Paradise (2015), and term caverns of all sizes on inclined to sub-vertical rock faces 'tafoni' (singular: tafone), and caverns on horizontal to slightly dipping surfaces 'weathering pits (gnammas)'. Where tafoni occur in groups, often covering whole bedrock outcrops, the elaborate, cell-like pattern is termed honeycomb structure (Mustoe, 1982; Turkington and Phillips, 2004). Kråkenes (61° 55′N, 05° 11′E), the north-western extending promontory of Vågsøy, features both tafoni and weathering pits (gnammas) on rock and boulder surfaces (Figs. 7 and 8). Weathering pits (0.1–0.7 m deep) and rounding of joints are widespread in the dominant augengneiss bedrock (Fig. 8e–f), whereas tafoni (up to 1.6 m deep) are restricted to the sliver of meta-gabbroic bedrock that crosscuts Kråkenes (Figs. 7 and 8a–c; Sigmond, 1992).

Grussic saprolite is observed at several localities on Vågsøy. A locality at Movatnet (3.4 km to the southeast of Kråkenes at c. 300 m a.s.l., 62.011°N, 5.018°E; Fig. 7a) hosts a saprolite of inferred pre-Pleistocene age (Roaldset et al., 1982; Olesen et al., 2012), although it has not been dated. The grussic saprolite is developed in augengneiss and contains rounded corestones (Fig. 8d). The outcrop was visited in 2005 but is now inaccessible due to construction activities related to nearby wind turbines. The saprolite consists mainly of sand with <15% silt

and < 2% clay, and a clay mineralogy containing vermiculite, illite, smectite, plagioclase, amphibole, and quartz (Roaldset et al., 1982; Olesen et al., 2012). Meter-wide grussic saprolite bands within the local meta-gabbro are observed along roadcuts near Kråkenes village and lighthouse (Olesen et al., 2012; Supp. Fig. S2), and weathering products are incorporated into tills in the area (Longva et al., 1983; Roaldset et al., 1982).

The regional ice movement around Kråkenes during the Late Weichselian was towards NW (Mangerud et al., 1979; Nygård et al., 2004). The Scandinavian ice sheet margin had retreated inland of Kråkenes by ~15–17 ka based on ice-sheet wide (Hughes et al., 2016; Stroeven et al., 2016) and regional (Nygård et al., 2004) reconstructions, while the minimum deglaciation age is constrained locally by dating of organic deposits in Lake Kråkenes, which sets the onset of organic production to 12.3 ^{14}C ka BP (Mangerud et al., 1979), corresponding to ~13.9 cal. ka BP (Birks, 2000). Late-glacial paleoclimate studies record the existence of a cirque glacier feeding Lake Kråkenes during the Younger Dryas (Larsen et al., 1998; Bakke et al., 2009). The presence of a Younger Dryas cirque glacier implies that the equilibrium line altitude lowered about 700 m during that period. However, the cirque glacier did not cover any of the described weathered sites (Fig. 7a). Shallow marine sediments deposited during the Tapes transgression (c. 7 ka BP), delineate the post-glacial marine limit on the island at 7–9 m a.s.l. (Longva et al., 1983). The tafoni, weathering pits, and saprolite discussed in this paper occur above this marine limit and were not post-glacially submerged below sea level (Fig. 7b).

The present-day climate at Kråkenes is temperate oceanic (Köppen, 1936). At Kråkenes lighthouse, positioned at the tip of the peninsula (Fig. 7a), the mean MAT for the 1926–1972 measurement period was 7.3 °C. Seasonal temperature variations are small, with mean daily temperatures varying mostly between −2.3 and 16.7 °C (1st–99th percentile within 1956–1991 record). The area is influenced by prevalent strong winds from the S-WSW exceeding 10 m/s for more than 30% of time within the 1926–1991 record (www.senorge.no; www.met.no). Precipitation (MAP: 1192 mm; 1926–1972) falls dominantly as rain and is distributed throughout the year, with the driest months (Apr–Jul) receiving half of the precipitation of the wettest (Sep–Dec).
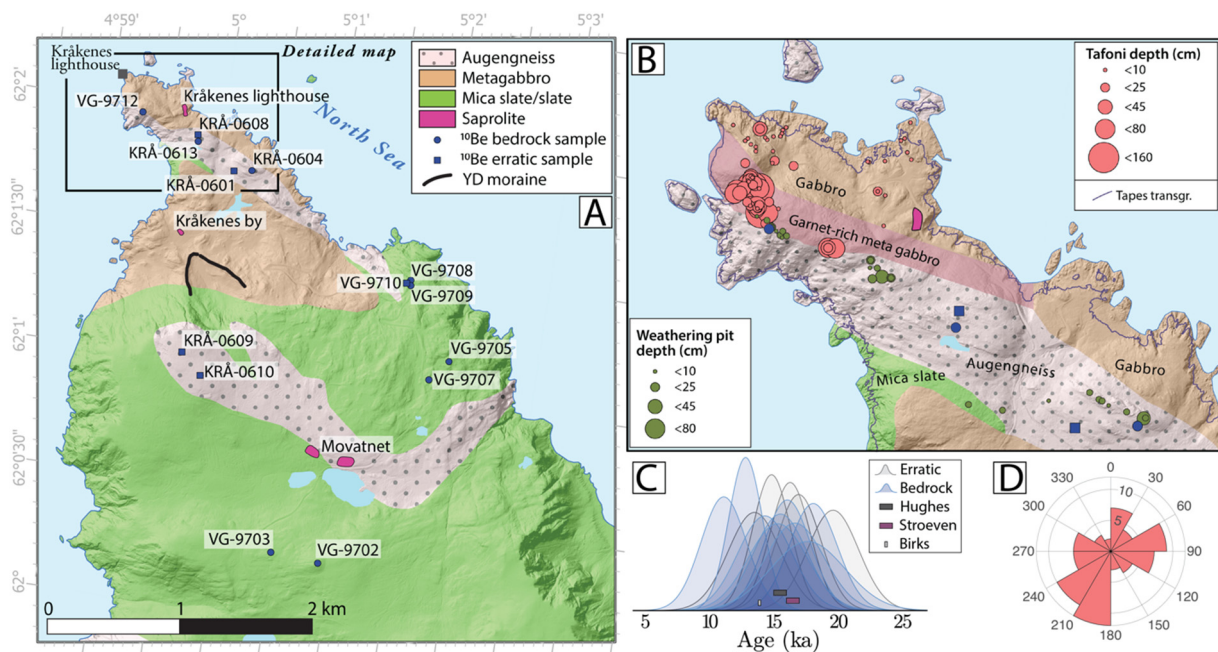

Fig. 7. Map of study area at A) NW Vågsøy and B) Kråkenes. C) Probability density functions of cosmogenic ^{10}Be ages from the nine bedrock (blue) and five erratic boulder (grey) samples compared to regional deglaciation estimates by Hughes et al. (2016) and Stroeven et al. (2016), and onset of organic production by Birks, 2000. D) Rose diagram shows aspects of tafoni (*n* = 73) measured in field.
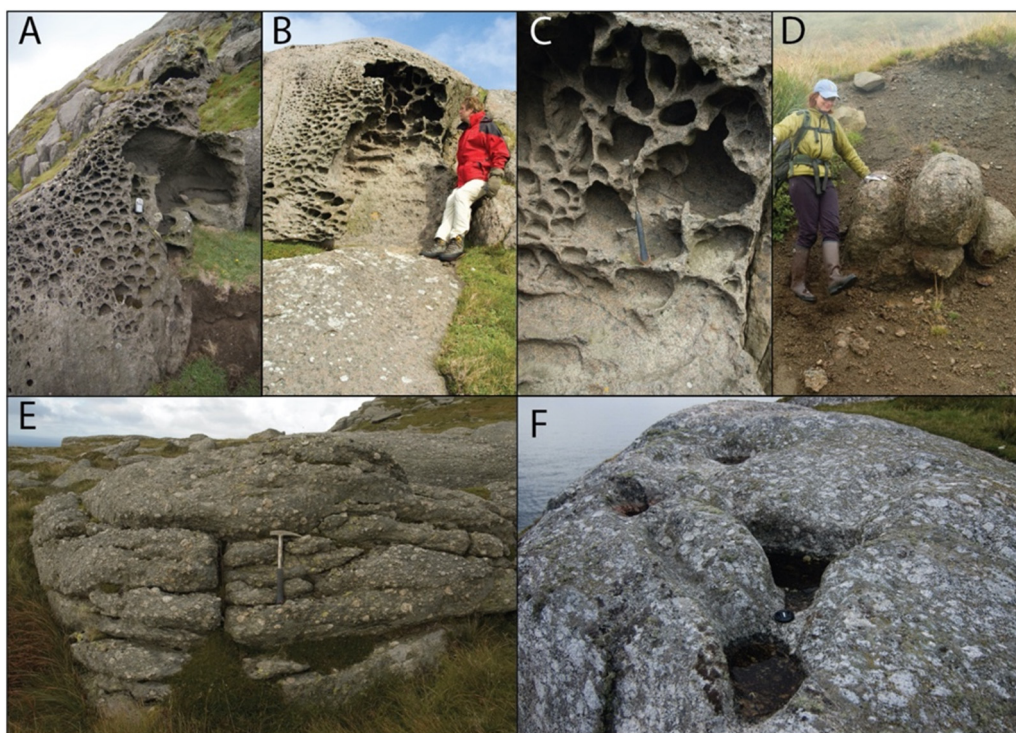
Fig. 8. Photographs from Kråkenes illustrating A–C) tafoni and honeycomb structures in meta-gabbro bedrock, D) saprolite with corestones at Movatnet, E) edge rounding of joints, and F) weathering pits (gnammas) in augengneiss. Note that tafoni-riddled surfaces occur adjacent to much smoother bedrock outcrops in A and B.
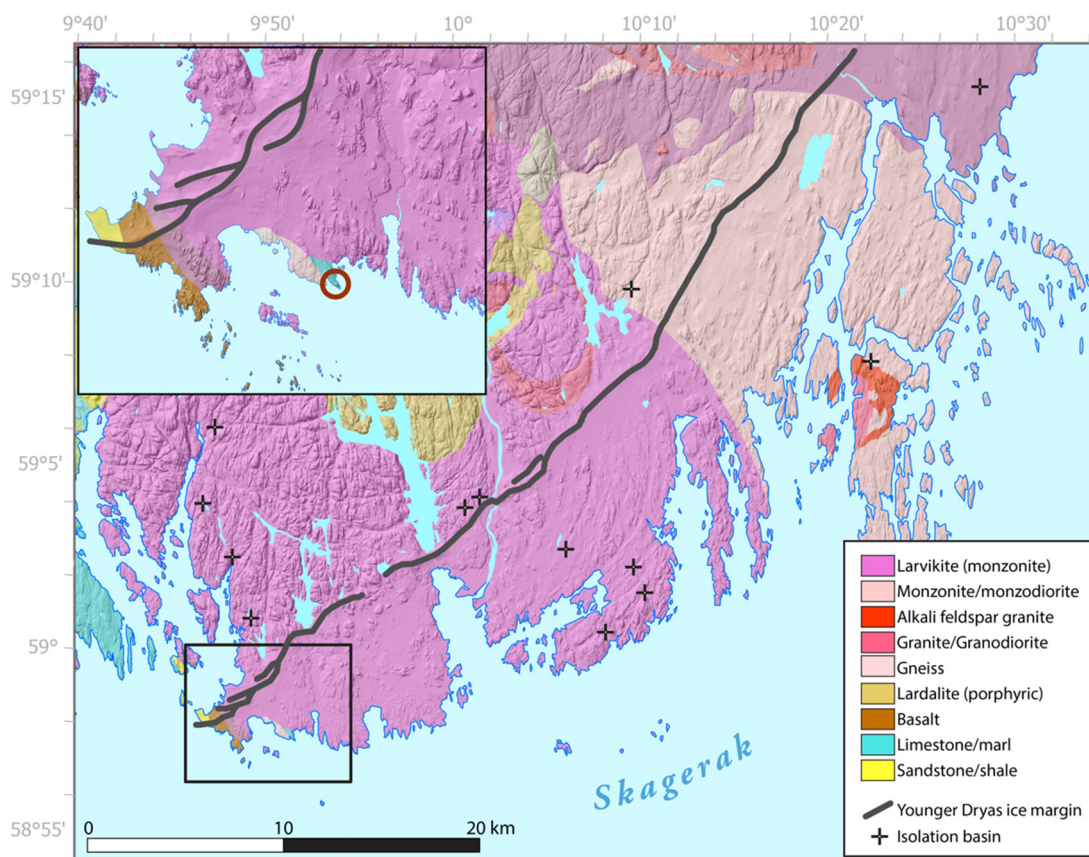

Fig. 9. Map of Nevlunghavn on the southern coast of Norway. The rectangle outlines the extent of the inset map. The studied weathering locality is encircled in inset figure. The locality is situated only a few kilometers outside of the Younger Dryas ice margin to the north-west.

2.3. Nevlunghavn – linear weathering grooves

The Nevlunghavn locality (58.96°N, 9.91°E) on the Norwegian south coast was first described by Reusch (1878), who reported surficial linear weathering features on "marly slate" bedrock outcropping along the shore (Figs. 9 and 10). Reusch (1878) noted that the weathering features could be postglacial, but remarked that an adjacent ~5 × 15 m large area within the same lithology shows no traces of weathering-induced surface roughness, but rather displays a smooth surface. He concluded that the smooth surface is a result of block removal by glacial plucking during the last glaciation, and that the linear weathering features on the immediately adjacent surface must have survived glacial erosion. A later review by Olesen et al. (2013) refers to the Reusch (1878) paper and suggests that this weathered surface could be a re-exhumed Mesozoic weathering surface.

We revisited the locality at Nevlunghavn, and augment Reusch's description of the linear weathering features with the following observations: (i) they dominantly consist of 0.5–5 cm wide, elongated, subvertical ridges separated by elongated grooves of similar widths and maximum depths up to ~5–7 cm, (ii) they strike subparallel to each other and roughly perpendicular to the shoreline, (iii) the boundary between the smooth and roughened surface strikes parallel with the grooves and with the lithological layering in the area, and (iv) the grooves are often continuous for up to tens of meters and generally display a regular pattern. However, some areas are dominated by shorter and more irregular features (Fig. 10b, d). The weathering features are reminiscent of 'rillenkarren' features described in literature (Bourke et al., 2007), which are associated with weathering by dissolution or preferential etching of less resistant minerals that accentuate compositional variations. Whereas the weathering features at Nevlunghavn fit this description, we note that the features appear to be strongly controlled by the parallel sub-vertical layering of the bedrock, and are more regular and parallel than rillenkarren described elsewhere (e.g. Bourke et al., 2007). Here, we apply the term
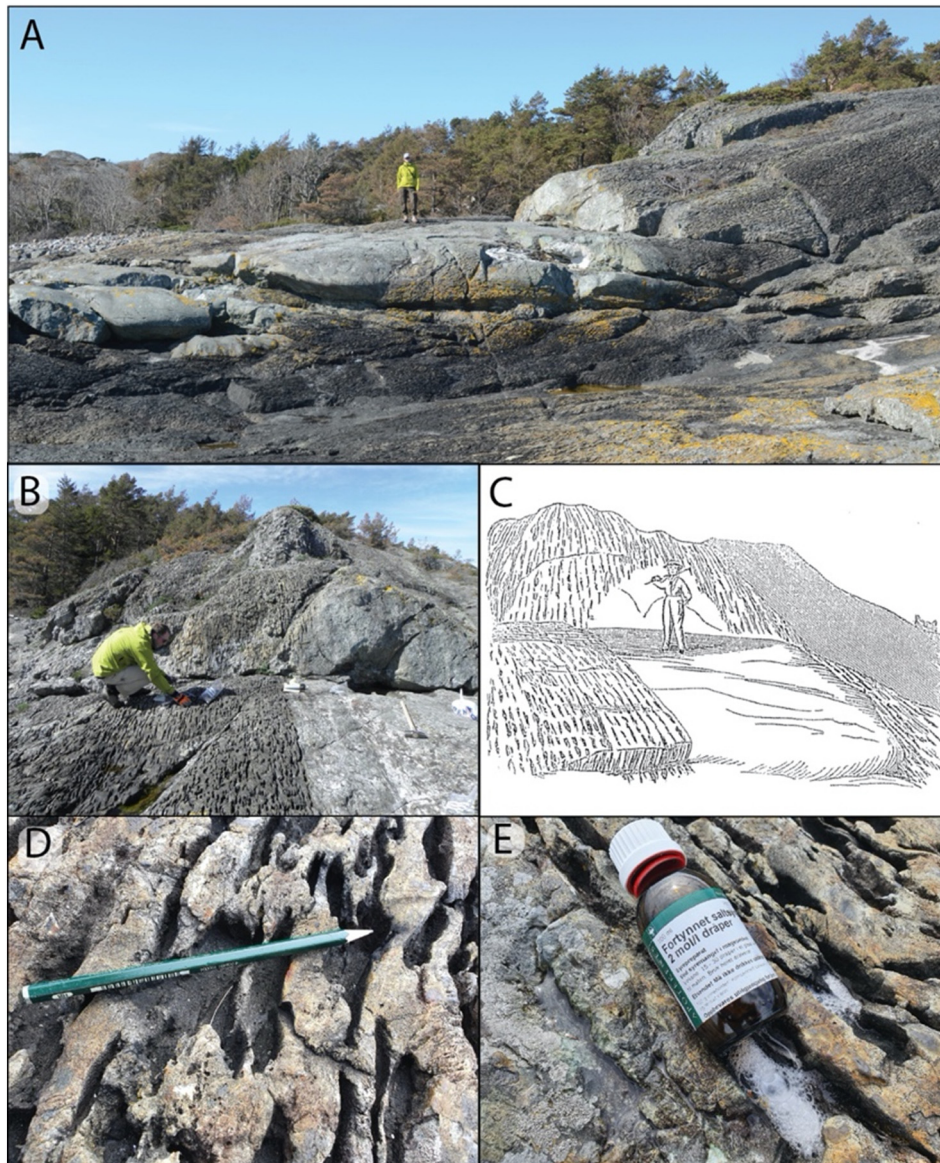

Fig. 10. Linear weathering grooves at Nevlunghavn. A) Overview photograph of the locality. The person is located on the smooth surface described in text, whereas linear weathering grooves cover most other surfaces on this outcrop. Note the apparent glacial sculpting of the outcrop resembling a roche moutonnée. B) Extraction of cosmogenic sample NEVL-04. Note the sharp transition between the smooth and linearly weathered surfaces with the boundary oriented parallel to the linear weathering grooves. C) Sketch of the locality from Reusch (1878), where the person is standing on the smooth surface, which Reusch interpreted to constitute the footprint of a glacially plucked slab. D) Close-up of linear weathering grooves cross-cut by a glacial groove oriented towards south, shown by the pencil. E) Dilute HCl acid reacts with rock within the linear weathering grooves (visible as white foam within depressions), while ridges between the weathering grooves, as well as the smooth surface in the lower left corner are non-reactive. The HCl bottle is about 8 cm tall.

'linear weathering grooves' to describe these features and the 'linearly weathered surface' to describe the area where they dominate the rock surface. The linear weathering grooves at Nevlunghavn are developed on a roof pendant of Silurian calcareous schist embedded within the Permian Larvik Plutonic Complex (Padget, 1999; Sunde et al., 2019). The bedrock surface is sub-planar with a <10° tilt towards the sea, but a ~1.5 m step in topography occurs ~20 m from the shoreline (Fig. 10a–c). Above this step the linear weathering grooves cover the entire surface (Fig. 10a–b). A ca. 30 cm deep circular pit with a diameter of about 1 m occurs on the smooth surface immediately below this step.

During the LGM, the Nevlunghavn locality was situated close to the head of the Norwegian Channel Ice Stream in the Oslofjord, which is today an area of widespread glacial scour (Reusch, 1878; Kleman et al., 2008). A reconstruction of ice-retreat indicates that the site deglaciated ~13–14 ka, and barely escaped cover by the Younger Dryas readvance, which reached a position 2.5 km northwest of the site (Fig. 9; Hughes et al., 2016; Stroeven et al., 2016). At the time of deglaciation, the area was submerged below sea level due to isostatic depression from ice-sheet loading. An initial rapid isostatic rebound was followed by transgression during the Younger Dryas due to renewed ice-sheet loading and gravitational attraction (Lohne et al., 2007). A relative sea level curve based on dating of isolation contacts in basins around Larvik indicates that the Nevlunghavn site emerged above sealevel within the last ~1–2 kyr (Figs. 9 and 11a; Sørensen et al., 2014). Since the LGM, Nevlungshavn has therefore only been exposed to subaerial weathering for the past ~1–2 kyr.

Presently, Nevlunghavn has a MAT of 7 °C (www.senorge.no) and the climate is temperate oceanic (Köppen, 1936). Within the last ten years, daily mean temperatures at nearby Svenner Fyr climate station (58.97°N, 10.15°E, 15 m a.s.l.) varied seasonally between −8.2 and 20.9 °C (1st–99th percentile). Precipitation (MAP of 1000–1500 mm a^{-1}) falls year-round with the driest months (Feb-June) receiving about half the precipitation of the wettest (Oct-Nov). Snowfall occurs mainly from Dec-Mar (Larvik and Hedrum Climate Stations).

3. Methods

3.1. Geomorphological mapping, sampling, and grain size analysis

At Bogvetten, we investigate the timing of glacial erosion, and thus maximum age of formation of the grussy saprolite, using ^{10}Be cosmogenic nuclide chronometry on the perched rock caps ($n = 3$; Figs. 4c–e; 5). The surface extent of saprolite at Bogvetten is mapped from aerial photographs where it appears brightly coloured, largely devoid of vegetation and bedrock structures (with exception of the pedestal rocks) compared to surrounding rock surfaces (Supp. Fig. 1a). Field observations were used to validate the aerial photograph mapping. To get a first-order impression of the degree of weathering of the saprolite at Bogvetten, we collected ten samples of in-situ material for grain size analysis (Figs. 2b and 3) and determined the mineralogical composition for a subset of four bulk saprolite samples by X-Ray Diffraction (XRD) analysis. To assess how the weathering of the dated summit saprolite compares to undated saprolite exposed in roadcuts and from an aggregate quarry in valleys adjacent to Bogvetten, we also performed grainsize analysis on seven samples, and XRD on two corestones, from these exposures (Fig. 2b). Two of these samples were from fracture planes within the saprolite (Fig. 6e). All saprolite samples were sufficiently disaggregated to be collected with a spoon. Grain size distributions determined by sieving (2–22 mm) and laser diffraction (<2 mm), and mineralogical determinations by XRD were performed at the Geological Survey of Norway (NGU) following standard procedures (Olesen et al., 2012).

To investigate the erosion history at Kråkenes, we applied in-situ ^{10}Be cosmogenic exposure dating of bedrock ($n = 9$) and boulder erratics ($n = 5$), matched with the known deglaciation age. Field mapping of tafoni and weathering pits was made using a hand-held GPS. We mapped the dimensions, positions, elevations, and aspects of tafoni and weathering pits to investigate potential links between weathering intensity and environmental and lithological factors such as orientation compared to the dominant wind-direction. The elevations were
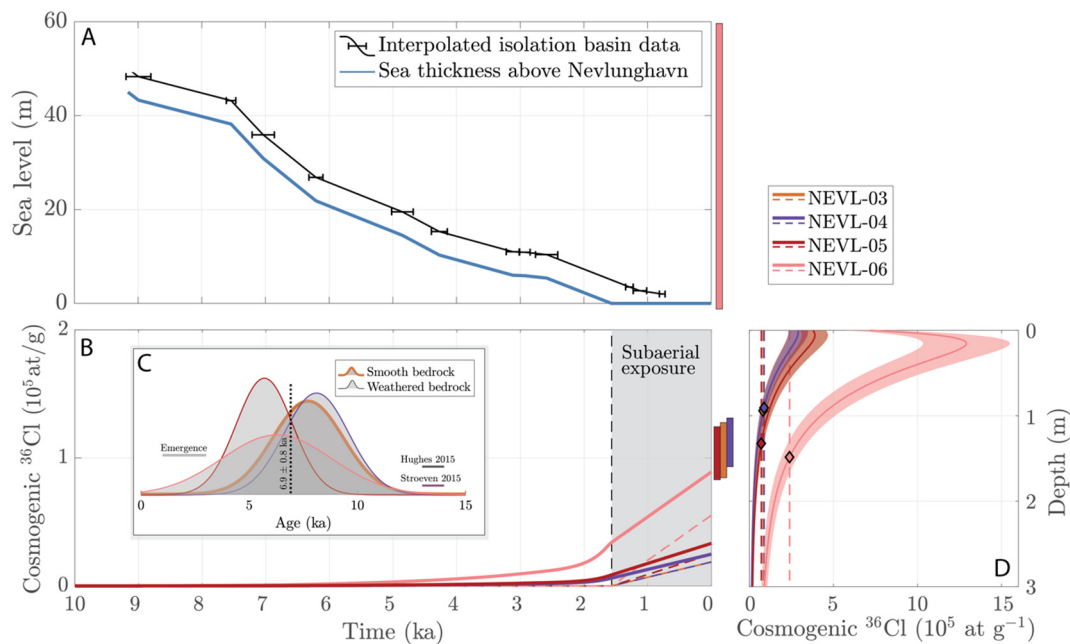

Fig. 11. Cosmogenic ^{36}Cl and sea-level emergence from Nevlunghavn. A) Sea level emergence for the Nevlunghavn site (5 m a.s.l.) based on isolation basin data (Sørensen et al., 2014; for locations see Fig. 9). B) Production of cosmogenic ^{36}Cl in the Holocene for the four cosmogenic samples with (full lines), and without (stippled lines) production through the sea water column. Bars to the right of the figure show measured ^{36}Cl concentrations for the samples (1σ including production rate scaling uncertainties. Note that the NEVL-6 bar is plotted to the same scale, although outside y-axis limits. C) Probability density functions of cosmogenic ^{10}Be ages from the four bedrock samples at Nevlunghavn compared to regional deglaciation estimates by Hughes et al. (2016) and Stroeven et al. (2016), and subaerial emergence interpolated from Sørensen et al. (2014). D) Cosmogenic ^{36}Cl inventories following 25 kyr of non-erosive exposure (estimated length of MIS3; best estimate depth profile ± 20% error envelope with depth below the ground surface) compared to ^{36}Cl inheritance in samples (stippled lines), with diamonds marking the intersection points at ~0.9–1.5 m depth.

Table 1
Bogvetten and Kråkenes apparent [10]Be exposure ages and sample data.

Sample ID	Type	Site	Elevation (m)	Latitude[*]	Longitude[*]	Thickness (cm)	Shielding correction	[10]Be Age (kyr)[**]	Internal unc.	External unc.
Bogvetten										
BOG01	Bedrock	Bogvetten	490	68.2133	16.0078	1.5	1.0	14.6	0.7	1.5
BOG02	Bedrock	Bogvetten	480	68.2139	16.0081	2.5	1.0	14.6	1.3	1.9
BOG03	Bedrock	Bogvetten	474	68.2142	16.0056	1.5	1.0	16.4	1.8	2.3
Kråkenes										
KRÅ-0601	Perched boulder	Kråkenes	55	62.0297	5.0024	2	1.0	17.0	0.9	1.7
KRÅ-0604	Bedrock, quartz vein	Kråkenes	68	62.0300	5.0051	1.5	1.0	18.1	1.0	1.9
KRÅ-0608	Bedrock, quartz vein	Kråkenes	71	62.0314	4.9968	2	1.0	16.1	1.1	1.8
KRÅ-0613	Erratic boulder on bedrock	Kråkenes	64	62.0317	4.9968	5	1.0	19.6	1.0	2.0
VG-9712[a]	Bedrock, augengneiss	Kråkenes	92	62.0331	4.9885	1	1.0	12.8	0.6	1.3
VG-9708	Bedrock, quartz vein	NW of Vardenibba	195	62.0241	5.0298	1	1.0	11.1	1.5	1.8
VG-9709	Bedrock, quartz vein	NW of Vardenibba	195	62.0241	5.0298	1	1.0	14.3	1.7	2.1
VG-9710	Boulder, quartz vein	NW of Vardenibba	195	62.0241	5.0298	1	1.0	13.5	1.7	2.0
VG-9705	Bedrock, quartz vein	S of Vardenibba	260	62.0192	5.0373	1	1.0	15.5	1.6	2.1
VG-9707	Bedrock, quartz vein	S of Vardenibba	278	62.0178	5.0348	1	1.0	15.3	1.9	2.3
VG-9702	Bedrock, quartz vein	Måsegga	433	62.0044	5.0231	1	1.0	16.7	1.8	2.3
VG-9703	Bedrock, quartz vein	Måsegga	390	62.0046	5.0162	1	1.0	17.7	2.5	2.9
KRÅ-0609	Boulder in till	Mehuken	433	62.0170	4.9994	2	1.0	14.8	0.7	1.5
KRÅ-0610	Boulder in till	Mehuken	420	62.0161	5.0019	3	1.0	16.3	0.6	1.6

[*] Determined by handheld GPS, reference datum WGS84.
[**] Age calculation of samples using the calculators formerly known as the CRONUS Earth calculators v 3.0.1. (Balco et al., 2008), with Scandinavian calibration dataset (Stroeven et al., 2015). All ages calculated with standard amosphere (ERA40atm), no erosion, a rock density of $2700 + -100$ kg m^{-3}, and the LSDn ('Sa') spallation scaling scheme, and are normalised to the "07KNSTD" ([10]Be) isotope ratio standardization. Internal uncertainties contain measurement uncertainties and counting statistics, while external uncertainties additionally comprise uncertainties related to production rate calibration and scaling.
[a] Corrected for postglacial surface erosion of 0.0002 cm a-1 based on relief of quartz veins in the area.

measured using an aneroid barometer with 1 m precision. Calibration of the aneroid was performed at sea-level every second hour. At each outcrop a subset of tafoni was measured, and approximate mean diameters and depths were calculated. All observations were plotted in a GIS and nearest distance to sea was calculated based on digitized shoreline from an orthorectified aerial photograph.

At Nevlunghavn, we explore the pre-glacial origin of the linear weathering grooves suggested by Reusch (1878) by measuring cosmogenic [36]Cl in the bedrock surfaces within the linearly weathered surface ($n = 3$), as well as within the adjacent smooth, non-weathered surface ($n = 3$) (Fig. 10b). Comparing the [36]Cl inventory across the weathering boundary is expected to reveal whether the smooth surface was glacially plucked, while the weathered surface was only surficially scoured.

3.2. Cosmogenic nuclide chronometry: apparent ages and [10]Be, [36]Cl measurements

To understand the rate of formation of the observed weathering phenomena, we apply cosmogenic nuclide chronometry to all our sites. Cosmogenic nuclides such as [10]Be ($T_{1/2} = 1.4$ Ma) and [36]Cl ($T_{1/2} = 0.3$ Ma) accumulate in surface rocks and sediment due to interactions with high-energy particles from space known as cosmic rays (Gosse and Phillips, 2001). Owing to the short penetration depth of the dominant spallation reaction (attenuation length: 150–230 g cm^{-2}; Marrero et al., 2016a), the inventory of cosmogenic nuclides in rock is highly sensitive to erosive surface processes as well as burial by sediment, snow, or ice cover. Given known surface production rates, the inventories of cosmogenic

nuclides can be converted to apparent exposure ages. We calculate apparent exposure ages assuming (i) no inherited nuclides from prior exposure, (ii) zero surface erosion, and (iii) no shielding by snow, soil or sediment cover (Tables 1–2). If all three of these assumptions are satisfied, apparent exposure ages reflect the true exposure age of a site, i.e., in this study the timing of last deglaciation. If glacial erosion during the last glaciation was insufficient to remove nuclides formed during previous exposure, the apparent ages will be older than the timing of last deglaciation, whereas post-glacial erosion or surface cover will lead to apparent ages younger than the last deglaciation. We compare apparent exposure ages from all our sites to the established timing of regional deglaciation to determine whether inherited nuclides from exposure prior to the Last Glacial Maximum are present in our samples. Inherited nuclides would indicate limited glacial erosion during recent glaciations (Ivy-Ochs and Briner, 2014; Andersen et al., 2018, 2020). The apparent ages thereby enables us to determine the time available for the observed weathering to develop.

We collected samples from bedrock at all three sites as well as glacially transported boulders resting on bedrock or till at Kråkenes (Tables 1–2, Supp. Tables S1–S3). The rock samples were processed according to standard procedures, but at different times and laboratories. Bogvetten samples were collected in 2016 and processed at the University of Bern after Akçar et al. (2017), [10]Be was measured at the Tandy AMS facility at ETH Zurich in 2017–19 (Müller et al., 2010; Christl et al., 2013) and normalised to in-house standards (S2007Nn and S2010N) that are calibrated against ICN-01-5-1 (Nishiizumi et al., 2007; Supp. Table S1). From Kråkenes, VG-samples were collected in

Table 2
Nevlunghavn apparent [36]Cl exposure ages and sample data.

Sample ID	Setting	Elevation (m)	Latitude[a]	Longitude[a]	[36]Cl age (kyr)[b]	Internal unc.	External unc.	Production on Ca (%)	Production on K (%)	Production on Cl (%)
NEVL-03	Smooth surface	5	58.9682	9.9057	7.7	1.5	1.6	83	0,3	16
NEVL-04	Weathered surface	5	58.9682	9.9057	8.1	1.4	1.5	76	4,7	19
NEVL-05	Weathered surface	5	58.9682	9.9057	5.7	1.2	1.3	35	39	25
NEVL-06	Weathered surface	5	58.9682	9.9057	6.3	2.3	2.5	14	13	73

[a] Determined by handheld GPS, reference datum WGS84.
[b] Apparent [36]Cl exposure ages calculated using the CRONUS Earth web calculators v 2.1 (Marrero et al., 2016b) with a global calibration dataset (Borchers et al., 2016). Internal uncertainties contain measurement uncertainties and counting statistics, while external uncertainties additionally comprise uncertainties related to production rate calibration and scaling.

1997 and processed and measured in 2000–2001 (except for VG-9712) according to the procedures described by Linge et al. (2006). $^{10}Be/^9Be$ ratios were obtained from the Tandetron AMS facility at Gif-sur-Yvette where measurements were done relative to NIST SRM 4325 with a nominal value of 2.68×10^{-11}. KRÅ-samples were collected in 2006 and processed and measured in 2006–2007, and VG-9712 was processed and measured in 2007–2008, according to procedures described by Fabel et al. (2012). $^{10}Be/^9Be$ ratios were obtained from the SUERC-AMS facility where measurements were done relative to NIST SRM 4325 with a nominal value of 3.06×10^{-11}. From these data, chemistry-blank corrected ^{10}Be concentrations were calculated (Supp. Tables S1 and S2). Because the bedrock lithology at the Nevlunghavn locality did not offer quartz for ^{10}Be analysis, we instead measured ^{36}Cl despite the more complicated production pathways of this nuclide (see discussion in Section 4.3). NEVL-samples were collected in 2015, processed at the University of Bern after Groos et al. (2021), and measured at Tandem AMS facility at ETH Zürich (Christl et al., 2013; Vockenhuber et al., 2019 (Supp. Table S3). To establish the ^{36}Cl production from low-energy neutrons, the bulk rock composition was analysed at Activation Laboratories Ltd. in Ontario, Canada (Supp. Table S3). With isotope dilution both total Cl and ^{36}Cl were determined from the same target at the ETH AMS facility (Synal et al., 1997).

Apparent ^{10}Be surface exposure ages were calculated using the calculators formerly known as the CRONUS Earth calculators v 3.0.1 (Balco et al., 2008), the Scandinavian calibration dataset (Stroeven et al., 2015), and the LSDn scaling scheme (Lifton et al., 2014; Table 1). Apparent ^{36}Cl exposure ages were calculated using the CRONUS Earth web calculators v 2.1 (Marrero et al., 2016b) with a global calibration dataset (Borchers et al., 2016), because a regional calibration dataset is not available for this nuclide (Table 2; Supp. Table S3).

4. Results

4.1. Bogvetten

All three bedrock samples from Bogvetten yield apparent ^{10}Be exposure ages overlapping within uncertainty with a weighted mean age of 15.0 ± 1.0 ka (1σ including production rate scaling uncertainties; Table 1). This age overlaps regional reconstructions of the timing of last deglaciation ~13–14 ka (Fig. 3; Hughes et al., 2016; Stroeven et al., 2016). The agreement between the three sample ages and with the regional deglaciation reconstructions implies that glacial erosion removed cosmogenic nuclides accumulated during previous exposure(s), to a depth of at least 1–2 m during the last glaciation (Andersen et al., 2018; Jansen et al., 2019). We cannot exclude that the Younger Dryas ice-margin re-advance briefly covered the summit of Bogvetten, but the agreement between our cosmogenic results and with the regional deglaciation reconstructions entails that such an ice cover would probably have been non-erosive.

The footprint of the mapped saprolite at Bogvetten is ~2.2 km², and another 0.5 km² area of saprolite occurs within the same granitic gneiss rock unit in the saddle towards Tiltvika (Fig. 2b). A third area of saprolite ~0.8 km² is exposed near the summit of the nearby mountain, Hatten (not visited in the field).

Field inspection of hand-specimens reveals that rocks hosting saprolite in the vicinity of Bogvetten all consist of medium-to-coarse-grained orthogneisses containing feldspar, quartz, biotite, and often hornblende, although the amount and distribution of biotite and hornblende differs among the suite of weathered rocks. Several, but not all, inspected saprolitic rock samples contain feldspar phenocrysts and former phenocrysts that have re-crystallised into a sugar-cube texture (Supp. Fig. S1). The inspected non-saprolitic granitoid surface rocks in the area are generally finer-grained, contain much less biotite and/or hornblende, and lack (re-crystallised) phenocrysts.

Grain-size analyses show that saprolite samples collected near the summit of Bogvetten ($n = 10$) consist of <0.4% clay and <3.4%

silt + clay, with a varying amount of sand and gravel (Fig. 12a). These distributions are comparable to samples ($n = 7$) collected along road cuts and in an aggregate quarry near Bogvetten, except for samples ($n = 2$) collected from fracture planes within these sections which contain up to 2.3% clay and 25% silt + clay (Figs. 4 and 12a). The mineralogical composition of the host rock, determined from two corestones and a pedestal surface sample (TY11), is dominated by feldspars, quartz, amphibole and mica, whereas the grussic saprolite additionally contains vermiculite (Fig. 12b–c). Increased field-assessed weathering intensity, estimated qualitatively from the coherence of the saprolite, is associated with a relative reduction of grain size and mica content, and an increase of vermiculite content (Fig. 12b–c). It thus appears that mica transforms to vermiculite as saprolitisation progresses.

4.2. Kråkenes

We analysed cosmogenic ^{10}Be in 14 samples from Kråkenes and NW Vågsøy, between 55 and 433 m a.s.l. (Table 1; Supp. Table S2). The ^{10}Be exposure ages from all 9 bedrock samples and 4 out of 5 boulder samples either overlap with the timing of regional deglaciation (15–17 ka, Nygård et al., 2004; Hughes et al., 2016; Stroeven et al., 2016) within uncertainty or are <4 kyr younger than this age (Fig. 7c). The older erratic boulder (KRÅ-0613: 19.6 ± 2.0 ka) contains some inherited cosmogenic nuclides accumulated either prior to, or during, glacial transport, whereas the two youngest bedrock ages (VG-9708 + 12: 11.1–12.8 ka) likely indicate surface erosion (~10–20 cm) following deglaciation. These two samples might alternatively indicate intermittent surface cover by snow and/or till, although burial only by snow would require on average 1.8–3.7 m wet snow for 6 months a year (Gosse and Phillips, 2001). The clustering of cosmogenic ages around the timing of the last regional deglaciation (Fig. 7c) indicates that cosmogenic nuclide inheritance from prior exposure is minimal, although there are large uncertainties associated with the ages. This implies that bedrock erosion depths during the last glacial period were at least 1–2 m (Andersen et al., 2018; Jansen et al., 2019).

Mapping of cavernous weathering features on Kråkenes revealed that both morphology and size are strongly dependent on lithology. Tafoni develop exclusively in medium-grained, equigranular meta-gabbroic rocks, typically on inclined surfaces, whereas weathering pits (gnammas) are developed in the local augengneiss (Figs. 7, 8). Incipient tafoni-like hollows were observed on meta-gabbroic rock outcrops (Supp. Fig. S2), but large tafoni are generally restricted to a garnet-rich meta-gabbro that is not delineated on the available bedrock map (Sigmond, 1992; Tveten et al., 1998), but was mapped in the course of this study (Fig. 7b). Well-developed tafoni are frequently localised, on some rock faces forming a dense (honeycomb) network, but with adjacent rock faces showing little to no sign of tafoni formation (Fig. 8a–b). Tafoni range in size from incipient forms a few cm deep, and up to 50–160 cm deep caverns with large overhanging sections and smaller tafoni sculpting all inside surfaces (Fig. 8 a-c). In some instances, adjacent tafoni with flat backwalls reach nearly the same depth, creating the impression that they have eroded back to the same level in the rock (Fig. 8c), although it is unclear whether this phenomenon is controlled by bedrock structures. In general, the garnet-rich meta-gabbro only has a weak foliation. The cm-thick walls separating alveoli were often sand-paper-like to touch, with sand-grains or small flakes of rock easily removed by hand. In a few cases, flaking is oriented along the rock foliation, creating a wavy texture at the bottom and sides of caverns (Supp. Fig. S2). The bottoms of some tafoni are covered in a thin green algae film or even cm-thick moss; however, this is not generally the case. While we observed tafoni across all aspects on the Kråkenes peninsula (Fig. 7d), they occur in particular high concentrations in a single south-west facing valley (Fig. 7b, d), where larger (decimeter to meter-scale) caverns are also more abundant. In a handful of instances, we observed rock horns and spurs protruding sub-vertical rock faces, reminiscent of collapsed former tafoni (Supp. Fig. S2).
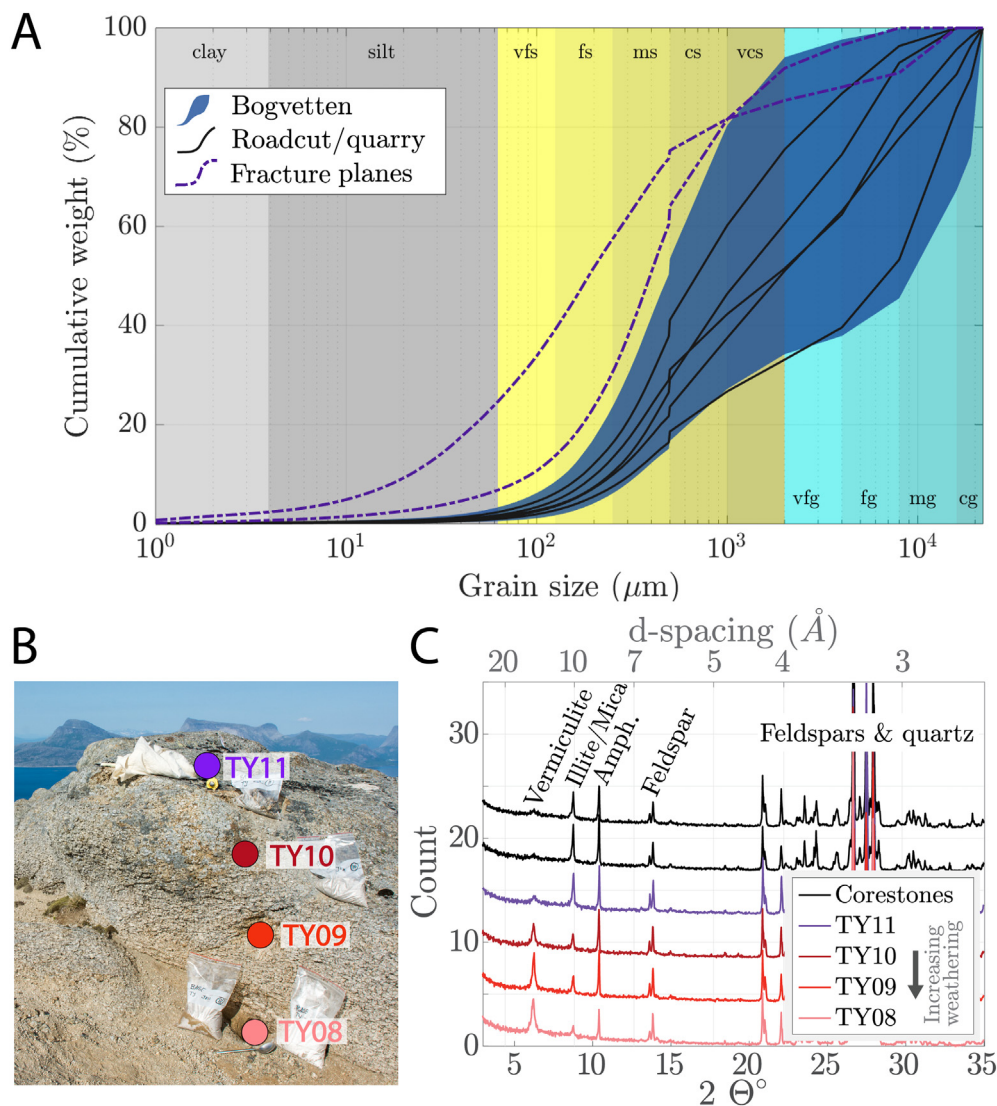
Fig. 12. A) Grainsize distributions of saprolite samples from Bogvetten (blue patch outline distribution of *n* = 10 samples; locations in Fig. 3), and from two roadcuts and a gravel pit in vicinity of Bogvetten (*n* = 7; locations in Fig. 2b). Fracture plane samples (purple dashed lines) are from within the roadcut and aggregate quarry saprolite exposures (Fig. 6e). Grey background colours are clay/silt, yellow colours are sand (vfs = very fine sand, fs = fine sand, ms = medium sand, cs = coarse sand, vcs = very coarse sand), and cyan are gravel (vfg = very fine gravel, fg = fine gravel, mg = medium gravel, cg = coarse gravel). B) Photo of samples retrieved from ~1 m high pedestal at Bogvetten summit (location in Fig. 3), the field-assessed weathering intensity (inverse of cohesiveness) increase towards the pedestal base. C) X-ray diffractograms of two corestones from roadcuts and the four pedestal samples shown in B, diffractograms are vertically offset for visibility. Amph. = Amphibole.

These structures did not seem to be associated with accumulations of rock debris at their bases, but vegetation made it difficult to determine this with certainty.

4.3. Nevlunghavn

Out of six bedrock samples from Nevlunghavn, we were only able to calculate apparent exposure ages for four samples, since two samples from the smooth surface showed natural $^{37}Cl/^{35}Cl$ ratios due to high total Cl (Supp. Table S3). The four remaining bedrock samples, one from the smooth and three from the linearly weathered surface, yield apparent ^{36}Cl exposure ages between 5.7 ± 1.3 and 8.1 ± 1.5 ka (Table 2). All apparent exposure ages overlap within 1σ and have a weighted mean age of 6.9 ± 0.8 ka. This implies that the entire outcrop, irrespective of the different surface weathering patterns, share a similar surface exposure and erosion history. However, the four samples have variable compositions and are consequently dominated by different ^{36}Cl production pathways (Table 2). Since the production pathways of ^{36}Cl are not equally well-constrained, the compositional differences

can, in principle, impede direct comparison between samples. This is particularly the case for low-energy thermal and epithermal neutron production on native ^{35}Cl (Marrero et al., 2016a). The dispersion of low-energy neutrons is highly affected by (fluctuations in) the water content within the rock, covering the rock surface, and in the vicinity of the sample site up to several hundred meters (Dunai et al., 2014). This problem is likely amplified at our coastal location (~5 m a.s.l.) where we expect great variations in water content both in the present due to wave- and tidally induced sea-level fluctuations, and in the past as the site emerged through the water-column. Fortunately, this complication is minimized for two of our samples that have relatively low and comparable Cl-content (~69 ppm Cl), similar geochemical composition (Supp. Table S3), and where only 16–19% of the total ^{36}Cl inventories stem from low-energy neutron production on native Cl (Table 2). One of these samples was collected from the smooth surface (NEVL-03; 7.7 ± 1.6 ka), whereas the other was collected from the linearly weathered surface (NEVL-04; 8.1 ± 1.5 ka). The similar apparent exposure ages of these two samples therefore clearly demonstrate that the cm-scale weathering at Nevlunghavn is unassociated with

differences in the duration of surface exposure of the smooth versus weathered surface.

The weighted mean apparent exposure age of the cosmogenic samples (6.9 ± 0.8 ka) postdates the regional deglaciation age of Nevlunghavn (13–14 ka) but predates the extrapolated surface emergence above sea level (~1–2 ka; Fig. 11c). The mismatch between apparent exposure ages and emergence from the sea (~5–6 kyr) can partially be explained by ^{36}Cl production during emergence through the water column (corresponding to ~0.5 kyr; Fig. 11b). Given the uncertainties related to the production rates and exposure history, we cannot reject the possibility that the remaining mismatch between calculated apparent ages and emergence from the sea could be caused by preservation of inherited cosmogenic nuclides produced prior to the LGM glaciation. The southern coast of Norway, including the site at Nevlunghavn, was probably ice free during most of Marine Isotope Stage 3 (MIS 3; ~60–30 ka; Mangerud et al., 2011). The Scandinavian Ice Sheet is inferred to have retreated to a restricted extent centered on the spine of the Scandinavian Mountain range during this period (Mangerud et al., 2011; Olsen, 2010; Kleman et al., 2021), while global eustatic sea level was >50 m lower than present during MIS 3 (Lambeck and Chappell, 2001; Siddall et al., 2003). Combined with the long duration of this interstadial (~30 kyr), leaving ample time for isostatic rebound, we infer that the site at Nevlunghavn was subaerially exposed during most of MIS 3 (>25 kyr, Wohlfarth, 2010). Hence, the relatively small amount of ^{36}Cl inheritance (corresponding to ~4.5–5.5 kyr of surface exposure) compared to the likely duration of exposure in Marine Isotope Stage 3 (~25 kyr) indicates that surface erosion of around 0.9–1.5 m (0.8–1.4 m assuming 10 mm ka^{-1} erosion during exposure, Supp. Fig. S4) took place during the LGM (Fig. 11d) and that the inherited nuclides may stem from muon production in the subsurface (Briner et al., 2016).

Since the cosmogenic results demonstrate that the differential weathering across the bedrock surface at Nevlunghavn is unrelated to exposure duration, we re-examined the local bedrock lithology across the boundary between linearly weathered and smooth rock. The rock has been mapped as Silurian limestone and slate embedded within Larvikite (Padget, 1999). Because this xenolith is 0.3 × 1 km in area, the whole outcrop is heavily influenced by contact metamorphism and hydrothermal alteration. We observe that the lithology is dominated by siliciclastic minerals, with calcite occurring only within the weathered rock surface. This was demonstrated when pouring dilute HCl acid over the rock in the field where a reaction was only observed on the linearly weathered surface, and within that area only in the weathered-out depressions/grooves, not on ridges (Fig. 10e). This experiment shows that the differential weathering probably reflects a lithological contrast. To substantiate this further, two samples were collected for thin section analysis, one within the weathered, and one within the smooth zone. Thin section and SEM analysis revealed that plagioclase feldspar and epidote dominate in both thin sections, with minor titanite, anorthite, and pyrite. In addition to this assemblage, the smooth surface also contains chlorite, and the linearly weathered surface also contains calcite, apatite, and muscovite. Both thin sections show linear zonation induced by mineral assemblage and grain size variations (Supp. Fig. S5). Younger veins infilled with plagioclase (both thin sections) and calcite (only in thin section from weathered surface) obliquely crosscut this zonation. Notably, in the linearly weathered rock, calcite appears as mineral grains within the rock matrix in some zones. Due to the high acid-solubility of calcite, the zonal distribution of this mineral may constitute a key factor for linear weathering groove development. The large compositional contrast between samples prepared for cosmogenic ^{36}Cl chemistry (Supp. Table S3) is probably also an effect of the mineral zonation.

We observed N-S oriented glacial indentations such as chatter marks (176–182°, $n = 5$) and grooves (170–184°, $n = 7$), on both the linearly weathered and smooth bedrock surfaces at Nevlunghavn. The directions are aligned with dominant deglacial flow lines (Bergstrøm, 2001) and obliquely cross-cut the linear weathering grooves (Fig. 10d).

5. Discussion

5.1. Weathering rates and timing

5.1.1. Bogvetten

Glacial landforms such as striae, chatter marks, whale backs, and roche moutonnées, generally develop on hard rock surfaces (Gilbert, 1906; Harris, 1943; Glasser and Bennett, 2004). Because these features occur on bedrock surfaces immediately adjacent to the saprolitic weathering mantle at Bogvetten, we infer that any overlying saprolite that may have formed prior to the last glaciation was glacially eroded. The formation of the present-day saprolite on Bogvetten followed the glacial sculpting of hard bedrock, and we can exclude the possibility that the grussic saprolite at Bogvetten is a basal remnant from truncation by glacial erosion of a formerly thick weathering profile. Our cosmogenic exposure dating results show that the grussic saprolite formed under climatic conditions that have prevailed during the ~15 kyr since the last deglaciation. Because samples were collected from remnant pedestal rock surfaces protruding up to ~1.5 m above the grussic saprolite (Figs. 4c–e; 5), we infer local saprolite formation- and erosion rates up to ~10 cm kyr^{-1} (based on a 1.5 m thick profile weathered and eroded away within 15 kyr, and assuming a top-down progression of weathering reaction fronts). This estimate (equal to 100 m Ma^{-1}) is 20 times higher than the highest Holocene weathering and erosion rates assessed from quartz-vein protuberances on ice-sculpted non-calcareous bedrock in Scandinavia (Dahl, 1967; André, 2002; Nicholson, 2008; Matthews and Owen, 2011), and 5–20 times higher than estimates of saprolite formation and erosion in the Appalachian Piedmont ranging from ~5–20 m Ma^{-1} (Pavich, 1989; Cleaves, 1993). Because the pedestal surfaces represent fragments of what appears to have been an undulating surface with m-scale relief at time of deglaciation (Fig. 5), we only have limited ability to assess the spatial variability of saprolite formation- and erosion across the summit of Bogvetten. Whereas saprolite formation- and erosion clearly progressed at slower rates in some areas where pedestal surfaces only protrude a few decimeters above the grussic saprolite (corresponding to rates of ~1 cm kyr^{-1}), the rates could have been faster in other areas where the absence of pedestal surfaces prevents direct estimates. We note that the rate of weathering front progradation is even higher than the weathering- and erosion estimates. Canyons incise the Bogvetten saprolite with canyon wall heights reaching up to ~5–10 m, exposing competent bedrock at their bases (Supp. Fig. 1d). If the scale of these incisions reflects the thickness of the saprolite down to fresh bedrock, post-glacial weathering front progradation of ~33–66 cm kyr^{-1} in excess of surface erosion is inferred.

The mineralogical composition of a pedestal surface at Bogvetten corresponds with corestones from adjacent valley roadcuts (Fig. 12d). Likewise, grainsize distributions of the saprolite at Bogvetten match saprolite samples from surrounding roadcuts and an aggregate quarry excavated into the saprolite, with the exception of samples collected from fracture planes within these sequences (Fig. 12a). To a first order, this indicates that the degree of weathering of different saprolite exposures in the area is comparable, and it is therefore possible that the roadside saprolite units also formed post-glacially, although we do not have direct age constraints for this locally. The lack of fine material and secondary minerals within the saprolite gives an indication that chemical weathering has not included intense mineral dissolution and particle size attrition, and that elemental mass loss is likely minor (Fig. 12). A more thorough investigation of the chemical and mineralogical properties is necessary to test the hypotheses of low mass loss and similar weathering characteristics between summit and roadside outcrops.

In summary, our results from Bogvetten demonstrate that several meters thick, grussy saprolite can form on glacially scoured rock surfaces within a postglacial timeframe (~15 kyr), even where the climate remains relatively cold. This setting offers a novel opportunity to

establish a direct link between saprolite development and climate, something that is notoriously difficult in regions that faced large climate fluctuations related to glacial cycles in the Quaternary (Migoń and Thomas, 2002).

5.1.2. Kråkenes

The cosmogenic nuclide ages from Kråkenes and NW Vågsøy cluster around the last deglaciation (15–17 ka), implying that widespread glacial erosion of at least 1–2 m took place during the last glacial period (Andersen et al., 2018; Jansen et al., 2019). However, the large uncertainties associated with these ages entails that we cannot exclude minor cosmogenic nuclide inheritance from prior exposures. The tafoni, weathering pit, and saprolite weathering sites were likely also glacially eroded during the last glacial period, although we did not obtain samples in the immediate vicinity to confirm this locally. The nearest cosmogenic samples to the tafoni, weathering pit, and saprolite weathering sites at Kråkenes are less than a few hundred meters away (Fig. 7b; VG-9712; KRÅ0604; KRÅ0608), while our nearest cosmogenic samples to the Movatnet saprolite are collected <1 km away (Fig. 7a; VG9702-03,05,07). The tafoni and weathering pits are generally shallow (mostly <50 cm, although the deepest tafone is 160 cm deep), and a few meters of erosion during the last glacial period would thus be sufficient to remove tafoni and weathering pits of similar sizes. If the tafoni formed entirely postglacially, they have deepened at rates of up to ~10 cm kyr^{-1} (based on the largest 160 cm deep cavern forming within 16 kyr). The recorded depths of the four deepest weathering pits (gnammas) in the augengneiss bedrock are 40–70 cm, corresponding to post-glacial deepening rates of 2.5–4.4 cm kyr^{-1}, which is 3–5 times faster than the formation of the deepest weathering pits (up to 8.2 cm) observed on ice-sculpted bedrock deglaciated ~10 ka in arctic northern Sweden (André, 2002).

Although our results indicate that the saprolite localities at Kråkenes and Movatnet (Fig. 7a) were at least surficially scoured by the last Scandinavian Ice Sheet, the age of saprolite formation cannot be firmly established by means of cosmogenic nuclide chronometry. Consequently, the possibility that these saprolites constitute the base of thicker, and older, saprolites cannot be excluded.

5.1.3. Nevlunghavn

The agreement between apparent exposure ages within the weathered and unweathered surface at Nevlunghavn shows that we can reject the hypothesis posed by Reusch (1878) - that the smooth region was glacially plucked during the last glacial period while the weathered surface underwent only slight glacial scouring. We find that both surfaces were eroded to a similar extent based on the comparable nuclide inventories.

The inference that the differential weathering at Nevlunghavn is not caused by differences in depth of glacial erosion is corroborated by observations in the field as well as our lithological investigations. Firstly, we observed multiple glacially produced indentations such as chatter marks, striae, and glacial grooves, on both the weathered and smooth bedrock surfaces (Fig. 10d; Supp. Fig. S3). We find it hard to envisage that subglacial conditions sufficient to produce these marks would leave adjacent delicate ridges on the weathered surface intact. Secondly, the depth of linear weathering grooves changes systematically with distance to the shoreline. In the tidal zone, weathering-groove depths are quite shallow (<3 cm) whereas they reach a maximum depth of ~5–7 cm at about 5–15 m from the shoreline, before becoming crumbly and irregular at the highest exposed parts and finally covered in vegetation inland. This apparent cycle of growth and destruction of the linear weathering grooves related to the length of exposure above present-day sea level implies that the linear weathering grooves are produced by present-day subaerial processes. Thirdly, our lithological investigations demonstrate an uneven distribution of calcite exclusively occurring in zones within the linearly weathered surface (Fig. 10e). We therefore propose that the linear weathering grooves: (i) are produced by surficial

dissolution of calcite by reaction with environmental acids; (ii) that the depth of dissolution weathering is self-regulated by collapse of the ridges and probably does not exceed the upper few decimeters of the surface, and; (iii) that glacial erosion of 0.8–1.5 m during the LGM (Fig. 11d; Supp. Fig. S4) was sufficient to remove any potentially pre-existing weathering grooves, creating a smooth, glacially scoured surface from where the present-day linear weathering grooves could develop. The similar cosmogenic nuclide inventories on both the smooth and linearly weathered surface furthermore demonstrates that the weathering process is not associated with large erosion rates. Based on the depths of the linear weathering grooves and duration since emergence above sea level we estimate that the linear weathering pattern develops at initial rates of ~5–7 cm kyr^{-1} that slow over time. This estimate is about two times higher than the maximum rate of Holocene weathering and erosion of calcitic schist bedrock along a lake shore in southern Norway (Owen et al., 2006).

5.2. Weathering mechanisms, lithological and environmental controls

Our investigation of three Norwegian sites shows that grussic saprolitisation in granitoid rocks, tafoni formation in garnet-rich metagabbro, weathering pit (gnamma) formation in augengneiss, and linear weathering groove formation in calcareous schist lithologies all can occur in cold temperate to subarctic coastal climates within timescales of 8–16 kyr. This diverse suite of weathering phenomena, although of limited spatial extent, demonstrates that weathering and erosion can take place at locally substantial rates (4–10 cm kyr^{-1}) in cold climates given the right circumstances. These circumstances may depend on local environmental conditions, lithological controls, or a combination of both. A comprehensive investigation and characterisation of the geochemical, mineralogical, and textural changes associated with the various weathering phenomena is necessary to establish causal relationships between processes and products. Although such an investigation is beyond the scope of the present paper, we will in the following summarize and discuss some basic observations that may indicate why the observed weathering phenomena have developed at these sites, but are not widespread across all formerly glaciated bedrock landscapes. We emphasise that these preliminary suggestions should be substantiated by further studies.

5.2.1. Bogvetten

5.2.1.1. Potential lithological factors. Grussic saprolites near Bogvetten and within the wider Lofoten-Vesterålen region preferentially occur in metamorphic plutonic rocks – granitic gneisses, monzonites, and granodiorites (Peulvast, 1985; Strømsøe and Paasche, 2011; Olesen et al., 2012), especially those that have undergone retrograde metamorphosis, introducing hydrous minerals such as biotite into otherwise relatively anhydrous plutonic rocks (Coint et al., 2020; N. Coint pers. comm.). Grussic saprolitisation of granitoid rocks has long been associated with the volumetric expansion that occurs with biotite oxidation (Wahrhaftig, 1965; Eggler et al., 1969; Isherwood and Street, 1976; Migoń and Thomas, 2002). Weathering of biotite to altered biotite occurs by oxidation of Fe(II) to Fe(III) and associated release of potassium from interlayer sites (Buss et al., 2008; White and Buss, 2014; Goodfellow et al., 2016). The ~5% volumetric expansion associated with oxidation of biotite may lead to intra/intergranular crack formation in medium- to coarse-grained rocks, which in turn may increase pore water flow and enable dissolution of relatively easily weatherable minerals such as plagioclase feldspar if weathering is allowed to proceed (Goodfellow et al., 2016). However, oxidation of iron in biotite can lead to disintegration of the rock into grus, even with minor mass losses (Goodfellow et al., 2016; Hayes et al., 2019). The saprolitisation at Bogvetten is associated with a reduction of mica and increase of vermiculite content (Fig. 12c), a change that could result from oxidation of the biotite. However, without establishing the causality, we cannot conclude

whether this reaction is responsible for saprolitisation. The recrystallised phenocrysts could be another component that aid the saprolitisation process at Bogvetten by increasing the density of grain boundaries and thereby inducing weaknesses in the rock. In general, prior magmatic, metamorphic, or perhaps hydrothermal alteration events generating pathways for circulation of oxygenated fluids, could be key to build susceptibility to biotite oxidation (Eggler et al., 1969; Kajdas et al., 2017).

5.2.1.2. Potential environmental factors. Grussic saprolites are thought to be most widespread in humid, temperate and tropical climates (Migoń and Thomas, 2002). Yet, we note that saprolites found in colder climates are often by default considered to be relict, which may in some cases veil the true environmental formation conditions. A range of environmental factors could potentially promote rapid saprolitisation at Bogvetten. In the following, we focus on the role of hydrology and frost weathering processes.

Because weathering reactions depend on the input of reagents and the removal of weathering products, stream incision sets the base level for saprolitisation through the control on the vadose zone (Goodfellow et al., 2014b; Rempe and Dietrich, 2014; Langston et al., 2015). The ephemeral streams eroding the saprolite at Bogvetten are incising steep, narrow canyons (Fig. 4f). Where we traced the streambed, it was often incised into competent bedrock, although some stretches were buried in grus or blocks (sometimes eroded corestones). The transition from bedrock in the streambed to saprolite along the canyon wall was surprisingly abrupt, occurring over <1–2 cm (Supp. Fig. S1). This indicates a correspondence between fluvial incision level and the base of the saprolite (Rempe and Dietrich, 2014; Riebe et al., 2017).

It was recently suggested that frequent low-magnitude subcritical stresses may govern mechanical damage accumulation in rock (Eppes and Keanini, 2017; Eppes et al., 2018). Potential damage-inducing factors encompass thermal and topography-related stresses as well as humidity/moisture availability, pore water chemistry and more (Eppes and Keanini, 2017). Since Bogvetten is situated at 68°N, it is relevant to consider the potential role of frost weathering processes. The MAT at Bogvetten is 3 °C, which theoretically allows for a high frost cracking intensity at shallow rock depths for sites with a thin (<10 cm) soil mantle (Andersen et al., 2015). But, Bogvetten mainly experiences seasonal freezing and sub-zero temperatures when the mountain is blanketed in snow, and a snow cover is known to effectively dampen frost cracking intensity (Andersen et al., 2015). Bogvetten is below the altitude limit for sporadic permafrost today (Gisnås et al., 2017), and probably was so throughout the Holocene (Lilleøren et al., 2012). Hence, we do not expect frost cracking to play a major role in the saprolitisation process in the Holocene or at present. However, from the deglaciation (~15 ka) until the Early Holocene the region was most likely situated in a permafrost environment (Alm, 1993; Birks et al., 2014). It is possible that periglacial processes could have impelled bedrock weakening during this (~5 kyr) period.

Neither hydrology, periglacial processes, snow cover, nor temperature variations, are unique to Bogvetten. Hence these environmental parameters cannot be the sole explanation for rapid saprolitisation. However, the combination of lithological and environmental factors could be key to condition rapid bedrock weathering at Bogvetten.

5.2.2. Kråkenes

5.2.2.1. Potential lithological factors. Lithology is a primary control on cavernous weathering at Kråkenes as underscored by the large differences in cavernous weathering development between adjacent meta-gabbroic rock-types and the augengneiss (Figs. 7 and 8). Even within the meta-gabbro, well-developed tafoni are often localised (Fig. 8a–b), potentially due to micro-lithological controls such as clustering of minerals. For example, we observed that clusters of garnets tended to form mm to cm-scale 'bumps' protruding rock surfaces (Supp. Fig. S2). Such small-scale variations could later be accentuated by positive, self-

organising feedbacks whereby the development of tafoni is self-sustainably increased (Turkington and Phillips, 2004). Globally, tafoni-structures are frequently reported from sandstone, limestone, or granitic gneiss lithologies according to a compilation of more than 50 described occurrences (Mustoe, 1982), whereas only one occurrence of tafoni in gabbro is listed in this compilation (Nichols, 1960). We are unable to identify a mechanism for why the garnet rich meta-gabbro at Kråkenes is especially susceptible to tafoni formation. It is often speculated that tafoni formation is conditioned by rock permeability that enables percolation of salty water through rock matrix, allowing intergranular growth of salt crystals that can break the rock apart (Mustoe, 1982; Turkington and Phillips, 2004; Mustoe, 2010; Sunamura and Aoki, 2011). However, the garnet-rich meta-gabbro at Kråkenes is apparently not more permeable than other similar rocks in Norway.

The observed occurrences of saprolite at Kråkenes are restricted to meta-gabbroic rock, whereas the nearby saprolite locality at Movatnet is developed in augengneiss (Roaldset et al., 1982; Olesen et al., 2012). Since our cosmogenic results do not yield a strict age control on the origin of these saprolites, we refrain from further speculations of their potential formation.

5.2.2.2. Potential environmental factors. Tafoni are often observed in rocks exposed to solutions of dissolved salts in environments characterised by cyclic wetting and drying such as in arid or coastal settings (Mustoe, 1982, 2010; Turkington and Phillips, 2004; Sunamura and Aoki, 2011). The formation of tafoni is thus often linked to mechanical disintegration by intergranular growth of salt crystals, where saline solutions seep into bedrock joints and evaporate (Cardell et al., 2003; Mustoe, 2010), although salt-induced chemical weathering has also been suggested (Young, 1987). The Kråkenes area on Vågsøy is influenced by ample sea spray and high winds. We therefore speculate that tafoni and weathering pits in this area have developed through salt weathering. Our initial hypothesis was that cavern size would decrease with increasing distance from the source of sea spray at the coast. However, we found no correlation between these parameters ($R^2 = 0.04$, $n = 73$; Fig. 13b). This indicates that salt supply may not be the limiting factor for cavernous weathering at Kråkenes. The volume of tafoni in the meta-gabbro is slightly more related to elevation above sea level, with generally larger pits at higher elevations ($R^2 = 0.19$, n = 73; Fig. 13a), although much scatter remains. Our current hypothesis is that either (i) decreasing sea spray at higher elevations allows the rock to dry more frequently than at lower elevations thereby enhancing crystallisation of salts in rock pores and fissures, and/or (ii) the large tafoni developed at a higher elevation area in the middle of Kråkenes (Figs. 7, 8b) are more exposed to wind-erosion (and potential salt deposition) because the principal aspect of this area (S-SW) coincide with the dominant wind direction at Kråkenes. However, large tafoni with other aspects also exist (Fig. 7d), and this explanation cannot stand alone. A number of additional factors may interplay to create favourable conditions for tafoni formation at Kråkenes. Differences in topographic position and thereby exposure to wind, rain, sea spray, and insolation probably control the number of wetting-drying cycles. Also, outcrop slope and drainage could be important due to the controls on surface runoff accumulation and thereby outwash of salts in this rainy environment. The latter is in line with our observation that tafoni mainly occur on isolated, relatively steep rock faces.

5.2.3. Nevlunghavn

5.2.3.1. Potential lithological factors. The development of linear weathering grooves on the shore at Nevlunghavn is closely linked to the structural bedrock features, inducing a sub-vertical layering of alternating more- and less calcite-rich zones. This zonation probably represents the initial bedding of layers with varying contents of siliciclastic and calcareous units, as is common for Lower Paleozoic rock units in the Oslo region (Bruton et al., 2010). The Permian magmatic intrusions, imbedding a
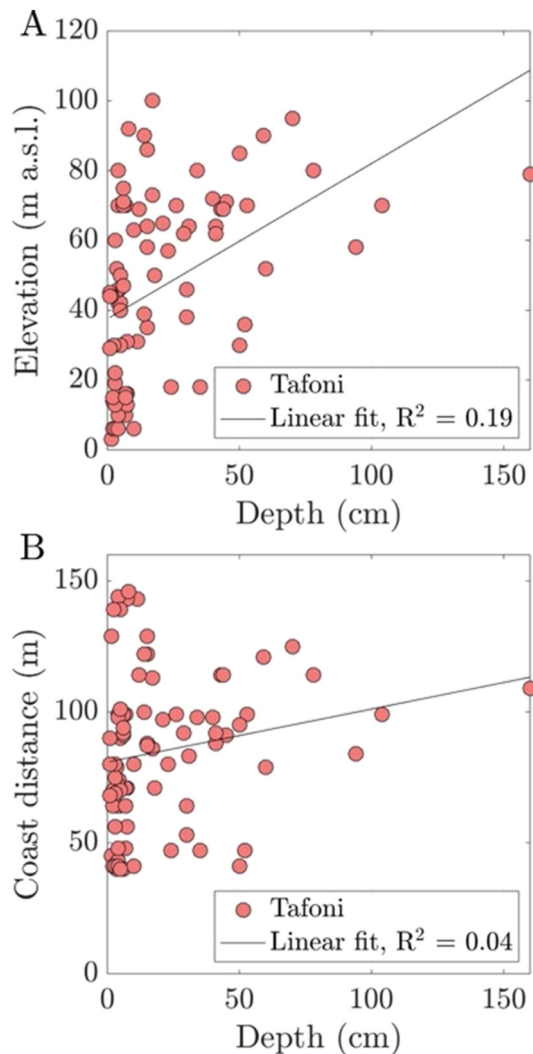
Fig. 13. Correlation between tafoni depth in meta-gabbro at Kråkenes and A) elevation, and B) distance from coastline.

xenolith of this Silurian host rock, led to contact metamorphism and hydrothermal alterations of the rock composition and mineralogy. We were unable to uncover whether the formation of adjacent calcite-rich (linearly weathered surface) and calcite-poor (smooth surface) rock units within the Nevlunghavn roof pendant is caused by the original sedimentary structure of the protolith or subsequent contact metamorphism.

5.2.3.2. Potential environmental factors. The existence of linear weathering grooves appears to be tied to the presence of calcium carbonate. It is therefore natural to assume that weathering and erosion of the grooves is instigated by dissolution via environmental acids. Potential acids could originate from dissolved CO_2 in precipitation or organic acids washed out from nearby vegetation. Given the coastal position of the site, and the history of emergence through sea level within the last few thousands of years, the potential role of marine and tidal processes should also be considered. However, given the preservation of mm-scale striae and chatter marks on many bedrock surfaces, wave-induced erosion must be minimal.

5.3. Implications for the landscape evolution and glacial erosion history

At high latitudes, glacial covers tend to show a selective linear, or patchy, erosive behaviour (Sugden, 1968; Stroeven et al., 2006), with subglacial preservation of delicate bedrock features and summit block-

fields through multiple glacial cycles (e.g., Stroeven et al., 2002; Fabel et al., 2002; Marquette et al., 2004; Briner et al., 2006; Goodfellow et al., 2014a; Margreth et al., 2016; Andersen et al., 2019). Such regions protected from glacial erosion delineate where former ice-sheets were thin, cold-based, and/or stagnant. However, interpreting specific landforms as relict pre-glacial landscape elements, and using those to make inferences about past glacial ice cover and basal glacial conditions, is questionable without quantitative constraints on the erosion history. Despite the occurrence of weathered landforms at the surface, the accordance between regionally reconstructed deglaciation ages and the exposure ages calculated from cosmogenic nuclide inventories shows that the last Scandinavian Ice Sheet eroded to depths of at least 1–2 m during the last glacial period at all three sites presented in this study. This demonstrates how distinguishing non-glacial landforms that can (re-)establish rapidly following glacial erosion has important implications for understanding the basal conditions of past ice-sheets. Notably, using the weathered localities investigated in this study to indicate a cold-based ice-sheet performing negligible glacial erosion is rejected by our results. Our findings thus have implications for the interpretation of weathering phenomena in Fennoscandia and other formerly glaciated landscapes, where weathered bedrock is often attributed to warmer-than-present paleoclimates, with only a subset of localities having direct or stratigraphic age control (Sturt et al., 1979; Lidmar-Bergström et al., 1997; Migoń and Lidmar-Bergström, 2001; Ebert et al., 2012; Gilg et al., 2013; Fredin et al., 2017). Many weathered bedrock localities are likely to have survived one or more periods beneath glacial ice, since they show more advanced chemical weathering and/or deeper weathering profiles than observed at the sites reported in this study (e.g., Lidmar-Bergström et al., 1997; Migoń and Lidmar-Bergström, 2001; Islam et al., 2002). However, in the absence of dating constraints, Holocene and/or interglacial weathering and glacial erosion of pre-Quaternary weathering profiles cannot be excluded.

The results presented in this paper demonstrates that weathering phenomena such as grussic saprolites, tafoni, and linear weathering grooves, are not unequivocal indicators of insignificant glacial erosion, instead they may in some circumstances indicate weak, easily weathered and eroded rocks, or post-glacial environmental conditions optimizing fast weathering through e.g., freeze-thaw cycles, high precipitation rates, or ample wind-borne salt spray. We wish to highlight the importance of carefully distinguishing between weathering phenomena developed on different lithologies, as well as separating the study of geochemical and mineralogical composition from dating of weathering (Bouchard and Jolicoeur, 2000). Whenever possible, numerical dating methods should be applied to infer weathering ages and erosion rates.

6. Conclusions

Although Fennoscandian landscapes are pervasively covered with signs of Quaternary glacial erosion, extensively weathered landforms also occur. Examples include in-situ weathered bedrock (saprolite), blockfields, and localised coastal weathering phenomena such as linear weathering grooves and tafoni. Despite their limited geographical extent, these weathering forms have been the foci of discussions on long-term landscape evolution and the relative imprints of glacial versus non-glacial processes in the Fennoscandian landscape for over a century. Multiple studies have suggested that weathering features such as saprolites or blockfields represent the scattered remains of widespread deep weathering mantles that covered the pre-Quaternary Fennoscandian landscape, with the implication that glacial erosion has been minor.

Here, we have applied cosmogenic nuclide chronometry to three coastal Norwegian localities that display grussic saprolite, tafoni, and linear weathering grooves. The chronometry demonstrates that (i) glacial erosion was sufficient to remove cosmogenic nuclides accumulated during previous exposures, and therefore the observed weathering phenomena do not indicate negligible glacial erosion, (ii) whereas these weathering phenomena were previously interpreted as having survived

(recent) glaciations, our cosmogenic nuclide chronometry indicates that they most likely formed after the last deglaciation, and (iii) weathering rates are conditioned by lithological and environmental factors and can be locally rapid (4–10 cm kyr^{-1}) even in cold temperate to subarctic climates. Based on these results, we caution against inferring weathering rates and ages from morphology and geochemistry alone and suggest that numerical dating techniques should be applied wherever possible.

CRediT authorship contribution statement

The study was conceptualized by OF and LR. Laboratory work and AMS analyses was performed by HL, EJB, SY, MC, CV, and NA. Data analyses by JLA, AM, OF, JCF, and TH. Manuscript preparation and revision by JLA, AM, OF, HL, BG, JCF, JK, TSo, EJB, TSc, RvdL, LR, TH, NA. Fieldwork by JLA, AM, OF, HL, BG, JCF, JK, EJB, TSc, RvdL, VB, LR. All authors approved the final version of the manuscript.

Declaration of competing interest

The authors declare that they have no known competing financial interests or personal relationships that could have appeared to influence the work reported in this paper.

Appendix A. Supplementary data

Supplementary data to this article can be found online at https://doi.org/10.1016/j.geomorph.2021.108003.

References

Akçar, N., Ivy-Ochs, S., Alfimov, V., Schlunegger, F., Claude, A., Reber, R., Christl, M., Vockenhuber, C., Dehnert, A., Meinert, R., Schlüchter, C., 2017. Isochron-burial dating of glaciofluvial deposits: primary results from the Alps. Earth Surf. Process. Landf. 42, 2414–2425.

Alm, T., 1993. Øvre Æråsvatn-palynostratigraphy of a 22,000 to 10,000 BP lacustrine record on Andøya, northern Norway. Boreas 22 (3), 171–188.

Andersen, J.L., Egholm, D.L., Knudsen, M.F., Jansen, J.D., Nielsen, S.B., 2015. The periglacial engine of mountain erosion–Part 1: rates of frost cracking and frost creep. Earth Surf. Dyn. 3 (4), 447–462.

Andersen, J.L., Egholm, D.L., Knudsen, M.F., Linge, H., Jansen, J.D., Pedersen, V.K., Xu, S., 2018. Widespread erosion on high plateaus during recent glaciations in Scandinavia. Nat. Commun. 9 (1), 1–7.

Andersen, J.L., Egholm, D.L., Knudsen, M.F., Linge, H., Jansen, J.D., Goodfellow, B.W., Fredin, O., 2019. Pleistocene evolution of a scandinavian plateau landscape. J. Geophys. Res. Earth Surf. 123 (12), 3370–3387.

Andersen, J.L., Egholm, D.L., Olsen, J., Larsen, N.K., Knudsen, M.F., 2020. Topographical evolution and glaciation history of South Greenland constrained by paired 26Al/10Be nuclides. Earth Planet. Sci. Lett. 542, 116300.

André, M.F., 2002. Rates of postglacial rock weathering on glacially scoured outcrops (Abisko-Riksgränsen area, 68° N. Geogr. Ann. Ser. B 64, 139–150.

Bakke, J., Lie, Ø., Heegaard, E., Dokken, T., Haug, G.H., Birks, H.H., Nilsen, T., 2009. Rapid oceanic and atmospheric changes during the Younger Dryas cold period. Nat. Geosci. 2 (3), 202–205.

Balco, G., Stone, J.O., Lifton, N.A., Dunai, T.J., 2008. A complete and easily accessible means of calculating surface exposure ages or erosion rates from 10Be and 26Al measurements. Quat. Geochronol. 3 (3), 174–195.

Ballantyne, C.K., 1998. Age and significance of mountain-top detritus. Permafr. Periglac. Process. 9 (4), 327–345.

Bergstrøm, B., 2001. Langesund 1712 I og Stavern 1812 IV – Kvartærgeologisk kart – M 1: 50 000. Norges geologiske undersøkelse. https://www.ngu.no/upload/Publikasjoner/Kart/KV50/langesund_stavern.pdf.

Birks, H.H., 2000. Aquatic macrophyte vegetation development in Kråkenes Lake, western Norway, during the late-glacial and early-Holocene. J. Paleolimnol. 23 (1), 7–19.

Birks, H.H., Aarnes, I., Bjune, A.E., Brooks, S.J., Bakke, J., Kühl, N., Birks, H.J.B., 2014. Lateglacial and early-Holocene climate variability reconstructed from multi-proxy records on Andøya, northern Norway. Quat. Sci. Rev. 89, 108–122.

Bøe, R., Fossen, H., Smelror, M., 2010. Mesozoic sediments and structures onshore Norway and in the coastal zone. Norges Geol. Unders. Bull. 450, 15–32.

Borchers, B., Marrero, S., Balco, G., Caffee, M., Goehring, B., Lifton, N., Stone, J., 2016. Geological calibration of spallation production rates in the CRONUS-Earth project. Quat. Geochronol. 31, 188–198.

Bouchard, M., Jolicoeur, S., 2000. Chemical weathering studies in relation to geomorphological research in southeastern Canada. Geomorphology 32 (3–4), 213–238.

Bourke, M.C., Brearley, J.A., Haas, R., Viles, H.A., 2007. A Photographic Atlas of Rock Breakdown Features in Geomorphic Environments.

Briner, J.P., Miller, G.H., Davis, P.T., Finkel, R.C., 2006. Cosmogenic radionuclides from fiord landscapes support differential erosion by overriding ice sheets. Geol. Soc. Am. Bull. 118 (3–4), 406–420.

Briner, J.P., Goehring, B.M., Mangerud, J., Svendsen, J.I., 2016. The deep accumulation of 10Be at Utsira, southwestern Norway: implications for cosmogenic nuclide exposure dating in peripheral ice sheet landscapes. Geophys. Res. Lett. 43 (17), 9121–9129.

Bruton, D.L., Gabrielsen, R.H., Larsen, B.T., 2010. The Caledonides of the Oslo Region, Norway–stratigraphy and structural elements. Nor. J. Geol. 90 (3).

Buss, H.L., Sak, P.B., Webb, S.M., Brantley, S.L., 2008. Weathering of the Rio Blanco quartz diorite, Luquillo Mountains, Puerto Rico: Coupling oxidation, dissolution, and fracturing. Geochim. Cosmochim. Acta 72 (18), 4488–4507.

Cardell, C., Rivas, T., Mosquera, M.J., Birginie, J.M., Moropoulou, A., Prieto, B., Van Grieken, R., 2003. Patterns of damage in igneous and sedimentary rocks under conditions simulating sea-salt weathering. Earth Surf. Process. Landf. 28 (1), 1–14.

Christl, M., Vockenhuber, C., Kubik, P.W., Wacker, L., Lachner, J., Alfimov, V., Synal, H.-A., 2013. The ETH Zurich AMS facilities: performance parameters and reference materials. Nucl. Instrum. Methods Phys. Res., Sect. B 294, 29–38.

Cleaves, E.T., 1993. Climatic impact on isovolumetric weathering of a coarse-grained schist in the northern Piedmont Province of the Central Atlantic states. Geomorphology 8 (2–3), 191–198.

Coint, N., Keiding, J.K., Ihlen, P.M., 2020. Evidence for silicate–liquid immiscibility in monzonites and petrogenesis of associated Fe–Ti–P-rich rocks: Example from the Raftsund Intrusion, Lofoten, Northern Norway. J. Petrol. 61 (4), egaa045.

Dahl, R., 1967. Postglacial micro-weathering of bedrock surfaces in the Narvik district of Norway. Geogr. Ann. 49 A, 155–166.

Dunai, T.J., Binnie, S.A., Hein, A.S., Paling, S.M., 2014. The effects of a hydrogen-rich ground cover on cosmogenic thermal neutrons: implications for exposure dating. Quat. Geochronol. 22, 183–191.

Ebert, K., Willenbring, J., Norton, K.P., Hall, A., Hättestrand, C., 2012. Meteoric 10Be concentrations from saprolite and till in northern Sweden: Implications for glacial erosion and age. Quat. Geochronol. 12, 11–22.

Eggler, D.H., Larson, E.E., Bradley, W.C., 1969. Granites, grusses, and the Sherman erosion surface, southern Laramie Range, Colorado-Wyoming. Am. J. Sci. 267 (4), 510–522.

Eppes, M.C., Keanini, R., 2017. Mechanical weathering and rock erosion by climate-dependent subcritical cracking. Rev. Geophys. 55 (2), 470–508.

Eppes, M.C., Hancock, G.S., Chen, X., Arey, J., Dewers, T., Huettenmoser, J., Whitten, J., 2018. Rates of subcritical cracking and long-term rock erosion. Geology 46 (11), 951–954.

Fabel, D., Stroeven, A.P., Harbor, J., Kleman, J., Elmore, D., Fink, D., 2002. Landscape preservation under Fennoscandian ice sheets determined from in situ produced 10Be and 26Al. Earth Planet. Sci. Lett. 201 (2), 397–406.

Fabel, D., Ballantyne, C.K., Xu, S., 2012. Trimlines, blockfields, mountain-top erratics and the vertical dimensions of the last British-Irish Ice Sheet in NW Scotland. Quat. Sci. Rev. 55, 91–102.

Fløistad, K.R., Laberg, J.S., Vorren, T.O., 2009. Morphology of Younger Dryas subglacial and ice-proximal submarine landforms, inner Vestfjorden, northern Norway. Boreas 38 (3), 610–619.

Fredin, O., Viola, G., Zwingmann, H., Sørlie, R., Brönner, M., Lie, J.E., Knies, J., 2017. The inheritance of a Mesozoic landscape in western Scandinavia. Nat. Commun. 8 (1), 1–11.

Gilbert, G.K., 1906. Crescentic gouges on glaciated surfaces. Bull. Geol. Soc. Am. 17 (1), 303–316.

Gilg, H.A., Hall, A.M., Ebert, K., Fallick, A.E., 2013. Cool kaolins in Finland. Palaeogeogr. Palaeoclimatol. Palaeoecol. 392, 454–462.

Gisnås, K., Etzelmüller, B., Lussana, C., Hjort, J., Sannel, A.B.K., Isaksen, K., Åkerman, J., 2017. Permafrost map for Norway, Sweden and Finland. Permafr. Periglac. Process. 28 (2), 359–378.

Glasser, N.F., Bennett, M.R., 2004. Glacial erosional landforms: origins and significance for palaeoglaciology. Prog. Phys. Geogr. 28 (1), 43–75.

Goodfellow, B.W., Stroeven, A.P., Fabel, D., Fredin, O., Derron, M.H., Bintanja, R., Caffee, M.W., 2014a. Arctic–alpine blockfields in the northern Swedish Scandes: late Quaternary–not Neogene. Earth Surf. Dyn. 2 (2), 383–401.

Goodfellow, B.W., Chadwick, O.E., Hilley, G.E., 2014b. Depth and character of rock weathering across a basaltic–hosted climosequence on Hawai'i. Earth Surf. Process. Landf. 39, 381–398.

Goodfellow, B.W., Hilley, G.E., Webb, S.M., Sklar, L.S., Moon, S., Olson, C.A., 2016. The chemical, mechanical, and hydrological evolution of weathering granitoid. J. Geophys. Res. Earth Surf. 121 (8), 1410–1435.

Gosse, J.C., Phillips, F.M., 2001. Terrestrial in situ cosmogenic nuclides: theory and application. Quat. Sci. Rev. 20 (14), 1475–1560.

Groom, K.M., Allen, C.D., Mol, L, Paradise, T.R., Hall, K., 2015. Defining tafoni: re-examining terminological ambiguity for cavernous rock decay phenomena. Prog. Phys. Geogr. 39 (6), 775–793.

Groos, A.R., Akçar, N., Yeşilyurt, S., Miehe, G., Vockenhuber, C., Veit, H., 2021. Non-uniform Late Pleistocene glacier fluctuations in tropical Eastern Africa. Sci. Adv. 7 (11), eabb6826.

Hall, A.M., 1986. Deep weathering patterns in north-East Scotland and their geomorphological significance. Z. Geomorphol. 30 (4), 407–422.

Hall, A.M., Ebert, K., Kleman, J., Nesje, A., Ottesen, D., 2013. Selective glacial erosion on the norwegian passive margin. Geology 41 (12), 1203–1206.

Harris Jr., S.E., 1943. Friction cracks and the direction of glacial movement. J. Geol. 51 (4), 244–258.

Hayes, J.L., Riebe, C.S., Holbrook, W.S., Flinchum, B.A., Hartsough, P.C., 2019. Porosity production in weathered rock: where volumetric strain dominates over chemical mass loss. Sci. Adv. 5 (9), eaao0834.

Hughes, A.L., Gyllencreutz, R., Lohne, Ø.S., Mangerud, J., Svendsen, J.I., 2016. The last Eurasian ice sheets–a chronological database and time-slice reconstruction, DATED-1. Boreas 45 (1), 1–45.

Isherwood, D., Street, A., 1976. Biotite-induced grussification of the Boulder Creek Granodiorite, Boulder County, Colorado. Geol. Soc. Am. Bull. 87 (3), 366–370.

Islam, M.R., Peuraniemi, V., Aario, R., Rojstaczer, S., 2002. Geochemistry and mineralogy of saprolite in finnish Lapland. Appl. Geochem. 17 (7), 885–902.

Ivy-Ochs, S., Briner, J.P., 2014. Dating disappearing ice with cosmogenic nuclides. Elements 10 (5), 351–356.

Jansen, J.D., Knudsen, M.F., Andersen, J.L., Heyman, J., Egholm, D.L., 2019. Erosion rates in Fennoscandia during the past million years. Quat. Sci. Rev. 207, 37–48.

Kajdas, B., Michalik, M.J., Migoń, P., 2017. Mechanisms of granite alteration into grus, Karkonosze granite, SW Poland. Catena 150, 230–245.

Kleman, J., Stroeven, A.P., Lundqvist, J., 2008. Patterns of Quaternary ice sheet erosion and deposition in Fennoscandia and a theoretical framework for explanation. Geomorphology 97 (1–2), 73–90.

Kleman, J., Hättestrand, M., Borgström, I., Fabel, D., Preusser, F., 2021. Age and duration of a MIS 3 interstadial in the Fennoscandian Ice Sheet core area–Implications for ice sheet dynamics. Quat. Sci. Rev. 264, 107011.

Knies, J., Vogt, C., Matthiessen, J., Nam, S.-I., Ottesen, D., Rise, L., Bargel, T., Eilertsen, R.S., 2007. Re-advance of the Fennoscandian Ice Sheet during Heinrich Event 1. Mar. Geol. 240, 1–18.

Köppen, W.P., 1936. Das geographische System der Klimate: mit 14 Textfiguren. Borntraeger.

Lambeck, K., Chappell, J., 2001. Sea level change through the last glacial cycle. Science 292 (5517), 679–686.

Langston, A.L., Tucker, G.E., Anderson, R.S., Anderson, S.P., 2015. Evidence for climatic and hillslope-aspect controls on vadose zone hydrology and implications for saprolite weathering. Earth Surf. Process. Landf. 40 (9), 1254–1269.

Larsen, E., Attig, J.W., Rune Aa, A., Sønstegaard, E., 1998. Late-glacial cirque glaciation in parts of western Norway. J. Quat. Sci. 13 (1), 17–27.

Lauritzen, S.E., Lundberg, J., 1999. Calibration of the speleothem delta function: an absolute temperature record for the Holocene in northern Norway. The Holocene 9 (6), 659–669.

Lidmar-Bergström, K., 1997a. A long-term perspective on glacial erosion. Earth Surf. Process. Landf. 22 (3), 297–306.

Lidmar-Bergström, K., Olsson, S., Roaldset, E., 1995. Relief features and palaeoweathering remnants in formerly glaciated Scandinavian basement areas. Palaeoweathering, Palaeosurfaces and Related Continental Deposits, pp. 275–301.

Lidmar-Bergström, K., Olsson, S., Olvmo, M., 1997b. Palaeosurfaces and associated saprolites in southern Sweden. Geol. Soc. Lond., Spec. Publ. 120 (1), 95–124.

Lifton, N., Sato, T., Dunai, T.J., 2014. Scaling in situ cosmogenic nuclide production rates using analytical approximations to atmospheric cosmic-ray fluxes. Earth Planet. Sci. Lett. 386, 149–160.

Lilleøren, K.S., Etzelmüller, B., Schuler, T.V., Gisnås, K., Humlum, O., 2012. The relative age of mountain permafrost—estimation of Holocene permafrost limits in Norway. Glob. Planet. Chang. 92, 209–223.

Linge, H., Brook, E.J., Nesje, A., Raisbeck, G.M., Yiou, F., Clark, H., 2006. In situ 10Be exposure ages from southeastern Norway: implications for the geometry of the Weichselian scandinavian ice sheet. Quat. Sci. Rev. 25, 1097–1109.

Lohne, Ø.S., Bondevik, S., Mangerud, J., Svendsen, J.I., 2007. Sea-level fluctuations imply that the Younger Dryas ice-sheet expansion in western Norway commenced during the Allerød. Quat. Sci. Rev. 26 (17–18), 2128–2151.

Longva, O., Larsen, E., Mangerud, J., 1983. Stad, skildring av kvartærgeologisk kart 1019 II-M 1: 50 000. Universitetsforlaget.

Mangerud, J., Larsen, E., Longva, O., Sønstegaard, E., 1979. Glacial history of western Norway 15000–10000 BP. Boreas 8 (2), 179–187.

Mangerud, J., Gyllencreutz, R., Lohne, Ø., Svendsen, J.I., 2011. Glacial history of Norway. Developments in Quaternary Sciences. Vol. 15. Elsevier, p. 279.

Margreth, A., Gosse, J.C., Dyke, A.S., 2016. Quantification of subaerial and episodic subglacial erosion rates on high latitude upland plateaus: Cumberland Peninsula, Baffin Island, Arctic Canada. Quat. Sci. Rev. 133, 108–129.

Marquette, G.C., Gray, J.T., Gosse, J.C., Courchesne, F., Stockli, L, Macpherson, G., Finkel, R., 2004. Felsenmeer persistence under non-erosive ice in the Torngat and Kaumajet mountains, Quebec and Labrador, as determined by soil weathering and cosmogenic nuclide exposure dating. Can. J. Earth Sci. 41 (1), 19–38.

Marrero, S.M., Phillips, F.M., Borchers, B., Lifton, N., Aumer, R., Balco, G., 2016a. Cosmogenic nuclide systematics and the CRONUScalc program. Quat. Geochronol. 31, 160–187.

Marrero, S.M., Phillips, F.M., Caffee, M.W., Gosse, J.C., 2016b. CRONUS-Earth cosmogenic 36Cl calibration. Quat. Geochronol. 31, 199–219.

Matthews, J.A., Owen, G., 2011. Holocene chemical weathering, surface lowering and rock weakening rates from glacially-eroded bedrock surfaces in an alpine periglacial environment, Jotunheimen, southern Norway. Permafr. Periglac. Process. 22, 279–290.

Migoń, P., Lidmar-Bergström, K., 2001. Weathering mantles and their significance for geomorphological evolution of central and northern Europe since the Mesozoic. Earth Sci. Rev. 56 (1–4), 285–324.

Migoń, P., Thomas, M.F., 2002. Grus weathering mantles—problems of interpretation. Catena 49 (1–2), 5–24.

Müller, A.M., Christl, M, Lachner, J., Suter, M., Synal, H.A., 2010. Competitive 10Be measurements below 1 MeV with the upgraded ETH-TANDY AMS facility. Nucl. Instrum. Methods Phys. Res., Sect. B 268 (17–18), 2801–2807. https://doi.org/10.1016/j.nimb.2010.05.104.

Mustoe, G.E., 1982. The origin of honeycomb weathering. Geol. Soc. Am. Bull. 93 (2), 108–115.

Mustoe, G.E., 2010. Biogenic origin of coastal honeycomb weathering. Earth Surf. Process. Landf. 35 (4), 424–434.

Nesje, A., Dahl, S.O., Linge, H., Ballantyne, C.K., Mccarroll, D., Brook, E.J., Yiou, F., 2007. The surface geometry of the last Glacial Maximum ice sheet in the Andøya-Skånland region, northern Norway, constrained by surface exposure dating and clay mineralogy. Boreas 36 (3), 227–239.

Nichols, R.L., 1960. Geomorphology of Marguerite Bay area, Palmer Peninsula, Antarctica. Geol. Soc. Am. Bull. 71 (10), 1421–1450.

Nicholson, D.T., 2008. Rock control on microweathering of bedrock surfaces in a periglacial environment. Geomorphology 101, 655–665.

Nielsen, S.B., Gallagher, K., Leighton, C., Balling, N., Svenningsen, L., Jacobsen, B.H., ... Lykke-Andersen, H., 2009. The evolution of western Scandinavian topography: a review of Neogene uplift versus the ICE (isostasy–climate–erosion) hypothesis. J. Geodyn. 47 (2-3), 72–95.

Nishiizumi, K., Imamura, M., Caffee, M.W., Southon, J.R., Finkel, R.C., McAninch, J., 2007. Absolute calibration of 10Be AMS standards. Nucl. Instrum. Methods Phys. Res., Sect. B 258 (2), 403–413.

NOAA National Geophysical Data Center, 2009. ETOPO1 1 Arc-Minute Global Relief Model. NOAA National Centers for Environmental Information Accessed [06.09.21].

Nygård, A., Sejrup, H.P., Haflidason, H., Cecchi, M., Ottesen, D., 2004. Deglaciation history of the southwestern Fennoscandian Ice Sheet between 15 and 13 14C ka BP. Boreas 33 (1), 1–17.

Olesen, O., Bering, D., Brönner, M., Dalsegg, E., Fabian, K., Fredin, O., Solbakk, T., 2012. Tropical weathering in Norway. TWIN Final Rep. 188.

Olesen, O., Pascal Kierulf, H., Brönner, M., Dalsegg, E., Fredin, O., Solbakk, T., 2013. Deep weathering, neotectonics and strandflat formation in Nordland, northern Norway. Nor. J. Geol. 93.

Olsen, L, 2002. Mid and late Weichselian ice-sheet fluctuations northwest of the Svartisen glacier, Nordland, northern Norway. Geol. Surv. Nor. Bull. 440, 39–52.

Olsen, L, 2010. A buried late MIS 3 shoreline in northern Norway-implications for ice extent and volume. Norges Geol. Unders. Bull. 450, 1–14.

Ottesen, D., Rise, L, Knies, J., Olsen, L, Henriksen, S., 2005. The Vestfjorden-Trænadjupet palaeo-ice stream drainage system, mid-norwegian continental shelf. Mar. Geol. 218 (1–4), 175–189.

Owen, G., Matthews, J.A., Shakesby, R.A., 2006b. Holocene chemical weathering on a calcitic lake shoreline in an alpine periglacial environment: Attgløyma, Sognefjell, southern Norway. Permafr. Periglac. Process. 17, 3–12.

Paasche, Ø., Strømsøe, J.R., Dahl, S.O., Linge, H., 2006. Weathering characteristics of arctic islands in northern Norway. Geomorphology 82 (3–4), 430–452.

Padget, P., 1999. Berggrunnskart; Langesund; 17121; 1:50 000; sort/hvitt. Nor. Geol. Unders. https://aps.ngu.no/pls/oradb/rf.Visdok?c_dokid=0000049586

Paradise, T.R., 2015. Tafoni and other rock basins. Reference Module in Earth Systems and Environmental Sciences. Elsevier https://doi.org/10.1016/B978-0-12-409548-9.09570-1.

Pavich, M.J., 1989. Regolith residence time and the concept of surface age of the Piedmont "peneplain". Geomorphology 2 (1–3), 181–196.

Pedersen, V.K., Huismans, R.S., Moucha, R., 2016. Isostatic and dynamic support of high topography on a North Atlantic passive margin. Earth Planet. Sci. Lett. 446, 1–9.

Pedersen, V.K., Knutsen, Å.R., Pallisgaard-Olesen, G., Andersen, J.L., Moucha, R., Huismans, R.S., 2021. Widespread glacial erosion on the scandinavian passive margin. Geology https://doi.org/10.1130/G48836.1.

Peulvast, J.P., 1985. In situ weathered rocks on plateaus, slopes and strandflat areas of the Lofoten-Vesterålen, North Norway. Fennia-Int. J. Geogr. 163 (2), 333–340.

Peulvast, J.P., 1986. Structural Geomorphology and Morphological Development in the Lofoten–Vesterålen area, Norway.

Peulvast, J.P., 1988. Pre-glacial landform evolution in two coastal high latitude mountains: Lofoten-Vesterålen (Norway) and Scoresby Sund area (Greenland). Geogr. Ann. Ser. B 70 (4), 351–360.

Rempe, D.M., Dietrich, W.E., 2014. A bottom-up control on fresh-bedrock topography under landscapes. Proc. Natl. Acad. Sci. 111 (18), 6576–6581.

Reusch, H.H., 1878. Iagttagelser over isskuret Fjeld og forvitret Fjeld. Christiania Videnskabs-Selskabs Forhandlinger. 7, pp. 1–28.

Riebe, C.S., Hahm, W.J., Brantley, S.L., 2017. Controls on deep critical zone architecture: a historical review and four testable hypotheses. Earth Surf. Process. Landf. 42 (1), 128–156.

Roaldset, E., Pettersen, E., Longva, O., Mangerud, J., 1982. Remnants of preglacial weathering in western Norway. Nor. Geol. Tidsskr. 62 (3), 169–178.

Schermer, E.R., Redfield, T.F., Indrevær, K., Bergh, S.G., 2017. Geomorphology and topography of relict surfaces: the influence of inherited crustal structure in the northern Scandinavian Mountains. J. Geol. Soc. 174 (1), 93–109.

Siddall, M., Rohling, E.J., Almogi-Labin, A., Hemleben, C., Meischner, D., Schmelzer, I., Smeed, D.A., 2003. Sea-level fluctuations during the last glacial cycle. Nature 423 (6942), 853–858.

Sigmond, E.M.O., 1992. Bedrock map of Norway and adjacent ocean areas. Scale l 3.

Small, E.E., Anderson, R.S., Hancock, G.S., 1999. Estimates of the rate of regolith production using 10Be and 26Al from an alpine hillslope. Geomorphology 27 (1–2), 131–150.

Sørensen, R., Henningsmoen, K.E., Høeg, H.I., Gälman, V., 2014. Holocene landhevningsstudier i søndre Vestfold og sørsøstre Telemark–revidert kurve. Vestfoldbaneprosjektet. Arkeologiske undersøkelser i forbindelse med ny jernbane mellom Larvik og Porsgrunn kommune. Bind 1, 236–247.

Staiger, J., Gosse, J., Johnson, J., Fastook, J., Gray, J., Stockli, D., Stockli, L., Finkel, R., 2005. Quaternary relief generation by polythermal glacier ice. Earth Surf. Process. Landf. 30, 1145–1159.

Steer, P., Huismans, R.S., Valla, P.G., Gac, S., Herman, F., 2012. Bimodal Plio-Quaternary glacial erosion of fjords and low-relief surfaces in Scandinavia. Nat. Geosci. 5 (9), 635–639.

Stroeven, A.P., Fabel, D., Hättestrand, C., Harbor, J., 2002. A relict landscape in the Centre of Fennoscandian glaciation: cosmogenic radionuclide evidence of tors preserved through multiple glacial cycles. Geomorphology 44 (1–2), 145–154.

Stroeven, A.P., Harbor, J., Fabel, D., Kleman, J., Hattestrand, C., Elmore, D., Fredin, O., 2006. Slow, patchy landscape evolution in northern Sweden despite repeated ice-sheet glaciation. Spec. Pap. Geol. Soc. Am. 398, 387.

Stroeven, A.P., Heyman, J., Fabel, D., Björck, S., Caffee, M.W., Fredin, O., Harbor, J.M., 2015. A new scandinavian reference 10Be production rate. Quat. Geochronol. 29, 104–115.

Stroeven, A.P., Hättestrand, C., Kleman, J., Heyman, J., Fabel, D., Fredin, O., Caffee, M.W., 2016. Deglaciation of fennoscandia. Quat. Sci. Rev. 147, 91–121.

Strømsøe, J.R., Paasche, Ø., 2011. Weathering patterns in high-latitude regolith. J. Geophys. Res. Earth Surf. 116 (F3).

Sturt, B.A., Dalland, A., Mitchell, J.L., 1979. The age of the sub Mid-Jurassic tropical weathering profile of Andøya, Northern Norway, and the implications for the late Palaeozoic paleography in the North Atlantic region. Geol. Rundsch. 68, 523–542.

Sugden, D.E., 1968. The selectivity of glacial erosion in the Cairngorm Mountains, Scotland. Trans. Inst. Br. Geogr. 79–92.

Sunamura, T., Aoki, H., 2011. Application of an S-shaped curve model to the temporal development of tafoni of salt-weathering origin. Earth Surf. Process. Landf. 36 (12), 1624–1631.

Sunde, Ø., Friis, H., Andersen, T., 2019. Pegmatites of the Larvik Plutonic complex, Oslo Rift, Norway: field relations and characterisation. Nor. J. Geol. 99 (1), 93–111.

Synal, H.A., Bonani, G., Dobeli, M., Ender, R.M., Gartenmann, P., Kubik, P.W., Schnabel, C., Suter, M., 1997. Status Report of the PSI/ETH AMS Facility Nuclear Instruments and Methods In Physics Research Section B-Beam Interactions with Materials and Atoms. 123, pp. 62–68.

Turkington, A.V., Phillips, J.D., 2004. Cavernous weathering, dynamical instability and self-organization. Earth Surf. Process. Landf. 29 (6), 665–675.

Tveten, E., Lutro, O., Thorsnes, T., 1998. Geologisk kart over Noreg, berggrunnskart Ulsteinvik - 1:250.000. Noregs geologiske undersøking.

Vockenhuber, S., Miltenberger, K.-U., Synal, H.-A., 2019. 36Cl measurements with a gas-filled magnet at 6 MV. Nucl. Instrum. Methods Phys. Res. B 455, 190–194.

Wahrhaftig, C., 1965. Stepped topography of the southern Sierra Nevada, California. Geol. Soc. Am. Bull. 76 (10), 1165–1190.

White, A.F., Buss, H.L., 2014. 7.4-Natural weathering rates of silicate minerals. Treatise on Geochemistry, Second edition Elsevier, Oxford, pp. 115–155.

Wohlfarth, B., 2010. Ice-free conditions in Sweden during Marine Oxygen Isotope Stage 3? Boreas 39 (2), 377–398.

Young, A.R., 1987. Salt as an agent in the development of cavernous weathering. Geology 15 (10), 962–966.